ARTICLE IN PRESS

European Journal of Medicinal Chemistry xxx (xxxx) xxx

Contents lists available at ScienceDirect

European Journal of Medicinal Chemistry

journal homepage: http://www.elsevier.com/locate/ejmech

Optimization of novel oxidative DIMs as Nur77 modulators of the Nur77-Bcl-2 apoptotic pathway

Xuhuang Tu [a, 1], Xiaohui Chen [a, 1], Dongliang Zhang [a], Meichun Gao [a], Jingmei Liang [a], Guoliang Bao [a], Jie Zhang [a], Shuangzhou Peng [a], Xiaokun Zhang [a], Zhiping Zeng [a, *], Ying Su [a, b, **]

[a] School of Pharmaceutical Science, Fujian Provincial Key Laboratory of Innovative Drug Target Research, Xiamen University, Fujian, 361002, China
[b] NucMito Pharmaceuticals, Xiamen 361000, China

ARTICLE INFO

Article history:
Received 21 July 2020
Received in revised form
10 November 2020
Accepted 11 November 2020
Available online xxx

Keywords:
Nur77
Nur77 modulator
Nur77/Bcl-2 apoptotic pathway
Oxidized DIM
BI1071

ABSTRACT

Nur77, an orphan nuclear receptor, is a member of the nuclear receptor superfamily. Nur77 plays important roles in various biological processes. Previously we reported that BI1071(DIM-C-pPhCF$_3^+$MeSO$_3^-$), an oxidized form and methanesulfonate salt of (4-CF$_3$-Ph-C-DIM), can modulate Nur77's non-genomic apoptotic pathway through that Nur77 translocated from the nucleus to mitochondria to induce cytochrome *c* releasing and promote apoptosis of cancer cell. Here we report our efforts to further optimize BI1071. A series of BI1071 analogs were designed, synthesized and their apoptosis potency was systematically evaluated. Our preliminary structure-activity relationship study identified compound **10b** as a better modulator with strong binding to Nur77 and enhanced apoptotic activity. Binding studies demonstrated that **10b** could bind to its target Nur77 with an affinity value of 33 nM. Furthermore, mechanism studies reveal that **10b** acts as an anticancer agent by utilizing the Nur77-Bcl-2 apoptotic pathway.

1. Introduction

Nur77 (also known as TR3 and NGFI-B), a unique orphan member of the nuclear receptor superfamily and an immediate-early response gene, regulates diverse biological processes in response to various extracellular stimulations including growth factors, stress and death signaling [1,2]. Nur77 was originally recognized for its pro-active role in cell survival, proliferation and differentiation. It plays an important role in cell proliferation, differentiation, apoptosis, metabolism and immunity [3–11] of cancer cells. Overexpression of Nur77 in precancerous or several cancer cells, including colon, lung, and breast tumors [12–15], stimulates cell cycle progression and proliferation to maintain their growth and survival [16]. In contrast, low expression of Nur77 in cancer cells inhibits the growth, survival and migration of tumor [8,17–19].

Paradoxically, Nur77 also exerts death effect, perhaps being the most potent pro-apoptotic member in the nuclear receptor superfamily [1,13,14,20–22]. Nur77 expression is rapidly induced during apoptosis of immature thymocytes, T-cell hybridomas [23,24]. It is also a key mediator of apoptosis of cancer cells induced by chemotherapeutic agents [25–27]. The apoptotic effect of Nur77 appears to be clinically relevant, as gene expression profiles of human tumor samples reveal that downregulation of Nur77 is associated with metastasis of several primary solid tumors, including lung cancer, breast cancer, and prostate cancer [28]. In studying the molecular mechanism by which Nur77 triggers cell death program, we found that it could translocate from the nucleus to mitochondria, where it induces cytochrome *c* release and apoptosis in response to some apoptotic stimuli [29]. Our later studies demonstrated that the apoptotic effect of Nur77 is mediated by its interaction with Bcl-2, an anti-apoptotic Bcl-2 family member. The interaction between Nur77 and Bcl-2 converts Bcl-2 from an anti-apoptotic to a pro-apoptotic protein to induce apoptosis of cancer cells [30]. Overexpression of the anti-apoptotic protein Bcl-2 is commonly associated with various cancers including ER-positive [31], triple negative breast cancer (TNBC) [32], and colon cancer [33,34]. Thus, the ability of Nur77 to interact with Bcl-2 not only

* Corresponding author.
** Corresponding author. School of Pharmaceutical Science, Xiamen University, NucMito Pharmaceuticals, Xiamen 361000, China.
E-mail addresses: zengzhiping@xmu.edu.cn (Z. Zeng), ying.su@nucmito.com (Y. Su).
[1] These authors contributed equally to this work.

https://doi.org/10.1016/j.ejmech.2020.113020
0223-5234/

Please cite this article as: X. Tu, X. Chen, D. Zhang *et al.*, Optimization of novel oxidative DIMs as Nur77 modulators of the Nur77-Bcl-2 apoptotic pathway, European Journal of Medicinal Chemistry, https://doi.org/10.1016/j.ejmech.2020.113020

suppresses its anti-apoptotic function but also converts Bcl-2 into a pro-apoptotic molecule [29,30], providing an attractive strategy to induce apoptosis of TNBC and colon cancer cells with elevated levels of Nur77 and Bcl-2.

However, agents that can bind directly to Nur77 to trigger its mitochondrial localization and Bcl-2 interaction remain to be explored. Our group previously reported that an oxidation form of Ph-C-DIM (**BI1071**, DIM-C-pPhCF$_3^+$MeSO$_3^-$, Fig. 1B) binds Nur77 with submicromolar affinity, and effectively induces apoptosis of cancer cells in a Nur77-and Bcl-2-dependent manner [35]. As the first identified small molecule modulator of the Nur77-Bcl-2 apoptotic pathway, **BI1071** directly binds to Nur77 to induce Nur77 translocation from nuclear to mitochondria where it interacts with Bcl-2, resulting in the release of cytochrome *c* and apoptosis of cancer cells, which warrants further optimization.

Here we optimized the hit compounds targeting Nur77 as potent anticancer agent, **BI1071**, which belongs to oxidative DIMs. We carried out the chemical optimization on the phenyl ring and the N—H position of indolyl ring of **BI1071** (Fig. 3B) by rational drug design strategy (Figs. 2 and 3). Totally 36 novel oxidative DIM derivatives were designed, synthesized and bio-evaluated for their apoptosis activity in TNBC cell line MDA-MB-231 and colon cancer cell line HCT116. Moreover, the primary biological mechanism research, anticancer ability *in vivo*, and pharmacokinetic properties of final optimized compounds were studied.

2. The rational design of novel BI1071 derivatives targeting Nur77

Nur77 ligand binding pocket were occupied by bulk side chains [36], and no endogenous ligands have yet been identified. However, several grooves on the surface of the ligand binding domain (LBD) of Nur77 were identified as small-molecule binding regions [37—39]. Our previously work reported that **BI1071** could bind to the site B on Nur77-LBD, a surface groove formed by helices H1, H5, H7, H8, loops H1—H2, and H5—B1 (Fig. 2A) [35]. In this binding model, indole ring 1 interacts with His372 through hydrogen bonds, and the other indole ring 2 forms *pi-pi* stacking with Try453. Side chain of Lys456 interacts with phenyl ring of **BI1071** through *pi*-cation pattern. Furthermore, the phenyl ring and the indolyl rings make van der Waals interactions with the sidechains of Leu382, Leu373, Pro377, Ile463 and Val500 that form a hydrophobic environment. (Fig. 2B).

The docking model also suggests that some binding regions of the hit compound **BI1071** could be optimized by chemistry efforts. The phenyl group has only partial contacts with its surrounding groove (sub-region 1, Fig. 3A) formed by Thr379, Leu382, Ile463, and Lys456, implying that chemical substitutions on the phenyl moiety of **BI1071** could be explored. Thus, to study the spacious tolerability of sub-region 1, a variety of substituents possessing different electron properties and sizes were introduced to the

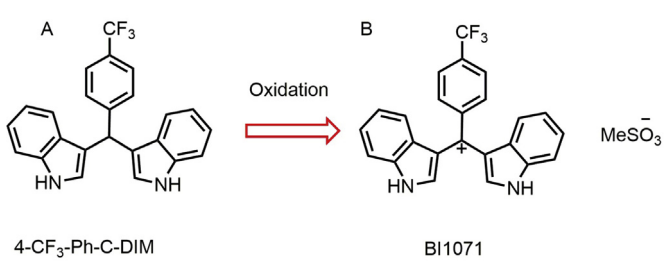

Fig. 1. (**A**) The structure of DIMs (4-CF$_3$-Ph-C-DIM). (**B**) The oxidative DIMs (**BI1071**, DIM-C-pPhCF$_3^+$MeSO$_3^-$).

ortho/*meta*/*para* positions of the phenyl ring (compounds **8a** - **8y**). In addition, we also studied the possibility of replacing the whole phenyl group with other aromatic rings (**9a** - **9f**).

We also found that the indolyl moiety 2 of **BI1071** lack good contacts with its surrounding hydrophobic region (sub-region 2, Fig. 3A) formed by helices 5, 7 and 8. To take advantage of this hydrophobic niche, several alkyl chains of different lengths were introduced on the N—H position of indole ring 2 of BI1071(**10b** - **10f**), aiming to enhance its binding affinity towards Nur77.

The PAINS (Pan analysis interfering compounds) evaluation was performed to exclude any compounds with potential issues of giving false positive results [40]. All of the designed compounds, **8a** — **8y**, **9a** - **9f**, and **10a** - **10f** passed the tests carried out using FAFDrugs4 (https://fafdrugs4.rpbs.univ-paris-diderot.fr/) or False Positive Remover (https://www.cbligand.org/PAINS/).

3. Chemistry

Preparation of the total 36 target compounds (**8a - 8y**, **9a - 9f**, and **10a - 10f)** was described in Scheme 1. Commercially available indole derivatives (**1a, 1b**) and aryl aldehyde derivatives (**2a** — **2y, 2a'** — **2f'**) were treated with hydrochloric acid to yield Ph-C-DIM (**3a** — **3y**, **4a** — **4f**, **5a**) [41]. For asymmetric Ph-C-DIM (**7a - 7f**), firstly, indole (**1a**) and 4-(trifluoromethyl)benzaldehyde (**2n**) were treated with tetramethylguanidine in H_2O to yield secondary alcohol (**6a**) [42]. The secondary alcohol is then treated with the indole derivatives (**1b - 1f**) in trifluoroethanol at 50 °C to obtain asymmetric Ph-C-DIM (**7a - 7f**) with good yield [43]. The Ph-C-DIM (**3a** — **3y**, **4a** — **4f**, **5a**, **7a - 7f**) was oxidized by pyridinium dichromate in the presence of methanesulfonic acid to yield Ph-C-DIM$^+$MeSO$_3^-$ (**8a - 8i, 8l - 8n**, and **10a - 10b**), and hydrochloric acid to yield Ph-C-DIM$^+$Cl$^-$ (**8a-1, 8f-1, 8j - 8k, 8n-1, 8o - 8y, 9a - 9f**, and **10c - 10f**).

Reagents and conditions: (a) HCl, MeOH, *r. t.*, (b) Pyridinium dichromate, acid, MeOH, *r. t.*, 1 h b$_1$, MeSO$_3$H, b$_2$, HCl (37%). (c) Tetramethylguanidine, H_2O, *r. t.*, 24 h. (d) 2,2,2-trifluoroethanol, 50 °C, 6 h.

4. Result and discussion

4.1. Apoptosis assay and SAR analysis

First, all the compounds were evaluated by poly (ADP-ribose) polymerase (PARP) cleavage assay for their apoptotic effects in MDA-MB-231 and HCT116 cell lines. The compounds' ability to induce apoptosis was quantitatively analyzed using the intensity ratio between the PARP cleavage band and the PARP band. Healthy, normal cells displayed no PARP cleavage or little PARP cleavage, while the apoptotic cells showed strong PARP cleavage. For easy analyses, each compound's apoptotic effect was compared to the apoptotic effect of **BI1071** (**8n**) of which the intensity ratio was set to 1 and relative intensity ratios were calculated. Western blot results and the corresponding quantitative calculation of the relative intensity ratio of PARP cleavage band/PARP band were shown in Fig. 4 - 8, and Tables S1—S6. We then analyzed the structure and apoptotic activity relationships (SAR) of the target compounds.

The organic-salt of Ph-DIM-C$^+$MeSO$_3^-$ consists of the cationic moiety of Ph-DIM-C$^+$ and the anion of MeSO$_3^-$, so, intuitively we first investigated whether using different anions for the organic-salt would have an impact on their apoptotic activities. Based on the synthesis feasibility, inorganic acid HCl and organic acid MeSO$_3$H were compared. For **8n** (**BI1071**), anions MeSO$_3^-$ (**8n**) and Cl$^-$ (**8n-1**) displayed similar apoptotic effect in MDA-MB-231 and HCT116 cell lines (Fig. 4). Similarly, for compound **8a** and **8f** (in MeSO$_3^-$ form), when the anion was Cl$^-$, not apparent differences were observed for their apoptotic effects (Fig. 4). Impact of different

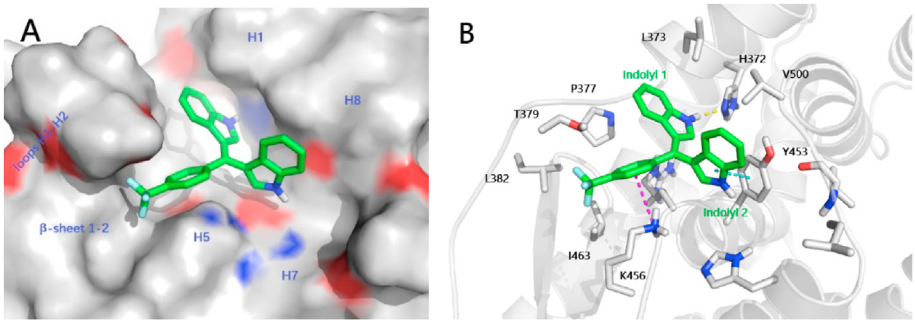

Fig. 2. The binding model of **BI1071** targeting Nur77. **A**. The location of **BI1071** on the surface of Nur77-LBD (3V3Q). The protein was represented as surface mode, and **BI1071** was shown as stick. The hydrophobic residues were colored in gray, and the polar residues were decorated with blue and red. **B**. the ligand-residue interaction of **BI1071** with Nur77-LBD. The H-bonds, *pi-pi* stacking and *pi*-cation interaction were shown in yellow dashed lines, cyan dashed lines, and magenta dashed lines, respectively. (For interpretation of the references to color in this figure legend, the reader is referred to the Web version of this article.)

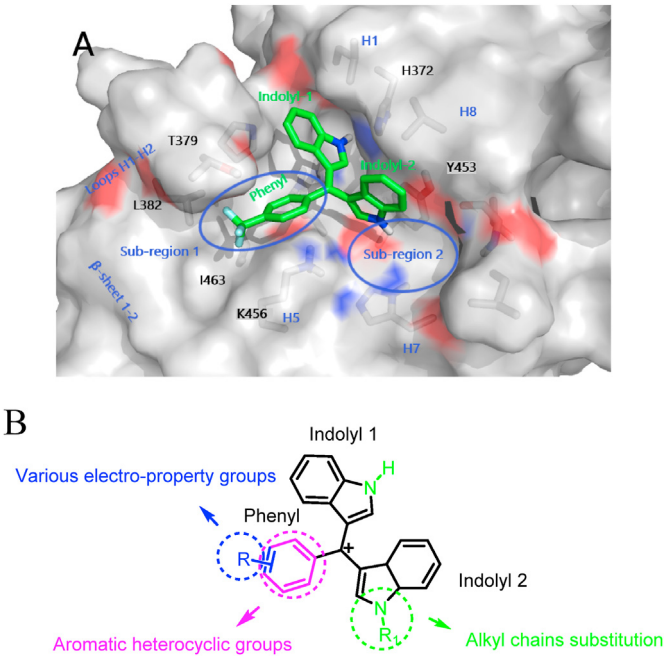

Fig. 3. Design strategy based on the **BI1071** binding profile. **A**. Surface binding analysis of **BI1071** in Complex with Nur77-LBD (3V3Q). The protein was represented as surface mode, and **BI1071** was shown as green stick. The hydrophobic residues were colored in gray, and the polar residues were decorated with blue and red, respectively. **B**. Design strategies used in this present study. (For interpretation of the references to color in this figure legend, the reader is referred to the Web version of this article.)

anions on the *in vitro* anticancer effect was also evaluated. The IC_{50} of compound **8n** was measured as 0.22 ± 0.10 μM in MDA-MB-231 cell line and 0.27 ± 0.10 μM in HCT116 cell line respectively. **8n-1** displayed almost the same anticancer effect with an IC_{50} value of 0.22 ± 0.09 μM in MDA-MB-231 and 0.26 ± 0.11 μM in HCT116 cell lines, respectively (Table 1). Taken together, these results indicated that the anion type $MeSO_3^-$ and Cl^- have no obvious different effects on the compounds' bioactivities. Therefore, either $MeSO_3^-$ or Cl^- was used to make BI1071 analogs, based on the synthesis feasibility.

Next, we examined the SAR at the phenyl group (-R) of the **BI1071**. A variety of substituents possessing different electron property were introduced to the *ortho*-, *meta*-, and *para*-positions of the phenyl ring of **BI1071** for structural optimization. For phenyl ring without $-CF_3$ substitution, **8a** (relative intensity ratio = 0.01, Table S2) showed significant decline in apoptotic activity in MDA-MB-231 cancer cell compared to reference compound **BI1071**(**8n**). Its activity wasn't rescued when the strong electron-donating group (-OH, **8f**) was used to replace the hydrogen group (**8a**). Increasing the steric effect at *para*-position by using a methoxy group (**8e**) or the replacement of the $-CF_3$ with methyl (**8b**), ethyl (**8c**) or *t*-butyl (**8d**) group did not gain any improvement on the apoptotic activity compared to **8n,** though they are more active than the hydrogen-substituted compound **8a** (Fig. 5A). Substituents with the electron-withdrawing natures, such as -Ph (**8g**), -Cl (**8h**), −F (**8i**), $-COOCH_3$ (**8j**), −COOH (**8k**) and $-NO_2$ (**8l**) at the *para*-position of the phenyl ring were explored. Unfortunately, all the above analogs demonstrated weaker apoptotic effect than **8n** (Fig. 5B). Hence, we can conclude that the $-CF_3$ group (**8n**) at the *para*-position of the phenyl group is the best choice. It was reported that fluorine substitution could enhance hydrophobic interactions and the lipophilicity of drugs [44,45]. In the binding model of BI1071 (Fig. 2), *para*-CF_3 group is surrounded by hydrophobic side chains of Leu 382, Ile463 and Lys456, which may explain why $-CF_3$ group worked the best at the *para*-position of the phenyl group.

Subsequently, we examined the impact of introducing substituents at the *meta*-position of the phenyl ring. Results of PARP cleavage assay showed that the electron donating group such as **8o** ($-CH_3$) or electron-withdrawing groups such as **8p** ($-OCH_3$), **8q** (-OH), **8r** (-Cl), and **8s** (-F) displayed sharp decrease in the apoptotic activity (Fig. 6). However, **8t** with *meta*-CF_3 substitution exhibited better apoptotic activity in MDA-MB-231 cell line (relative intensity ratio = 1.76, Table S4) compared to reference compound **8n**. Docking model showed that **8t** shared similar binding pose with **8n** (Fig. S1). Notably, the *meta*-CF_3 group of **8t** was buried and may make stronger interactions with the hydrophobic surroundings formed by Pro377, Leu382 and Ile463.

Similarly, introducing −OH, -Cl, or −F substituent at the *ortho*-position of the phenyl ring (**8u** (-OH), **8v** (-Cl) and **8w** (-F)) led to an activity reduction (Fig. 6). However, it is surprising to find that the *ortho*-CF_3 group (**8x**, $-CF_3$) or 2,4-*di*-CF_3 substituent (**8y**, 2,4-*di*-CF_3) were not favorable changes, acting differently from the *para*-CF_3 group or *meta*-CF_3 group (Fig. 6). In binding model of **BI1071**, the angle between phenyl ring and bis-indole rings 1 and 2 were 62.2° and 73.4°, respectively. And the ring angel of the two bis-indole rings is 80.6° (Fig. S2). However, in the minimized-energy conformation of **8x**, the ring angle were altered largely because of the steric hindrance of *ortho*-CF_3 group. The angle between phenyl ring and each bis-indole rings 1 and 2 were 79.0° and 80.5° respectively, and the ring angel of the two bis-indole rings was 57.0° (Fig. S2). It is likely due to this conformation change, **8x** could no longer dock well into the Nur77-LBD binding site.

Replacing the whole phenyl moiety with other aromatic heterocyclic groups, such as five-member ring (2-furyl **9a**, 2-thienyl

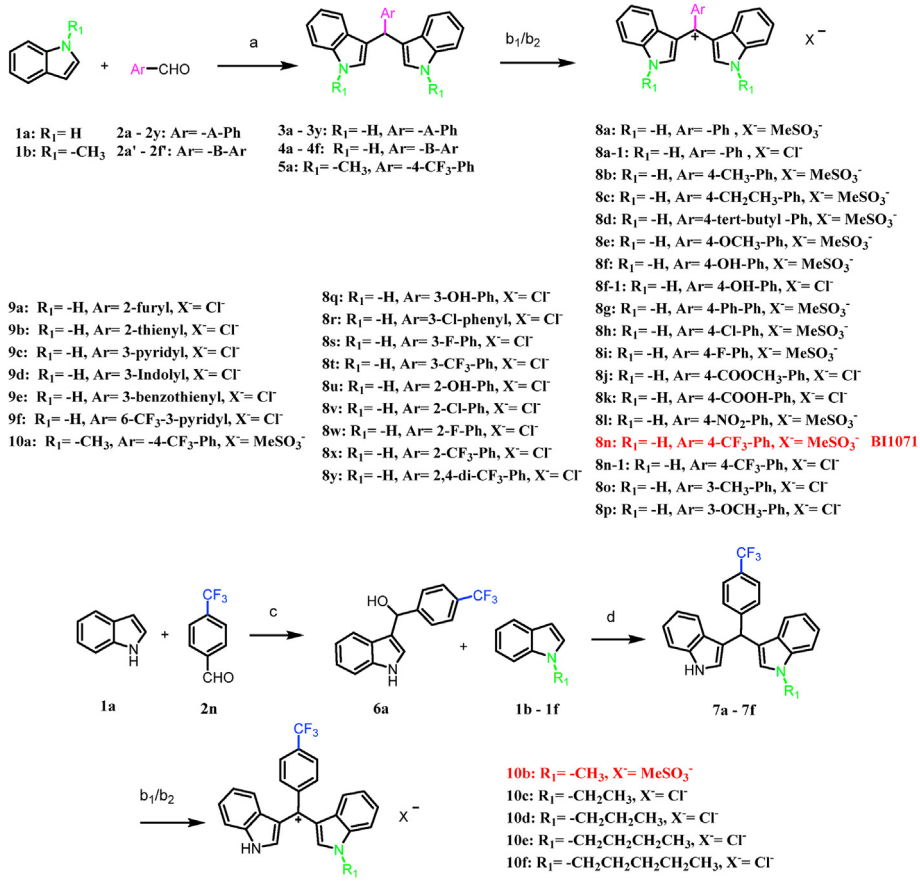

Scheme 1. Synthetic route of target compounds.

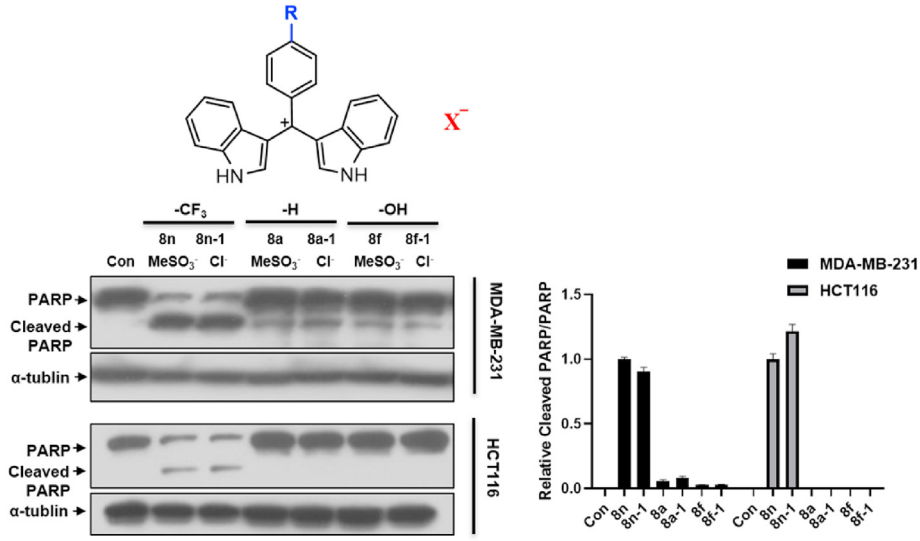

Fig. 4. Apoptotic activity of BI1071 derivatives with anion type of $MeSO_3^-$ or Cl^-. MDA-MB-231 and HCT116 cells were treated with compounds (0.5 μM) for 6 h, then PARP and cleaved PARP were analyzed by western blotting. The relative intensity ratio of PARP cleavage band/PARP band was counted and analyzed. Data are presented as mean ± SD.

9b), six-member ring (3-pyridyl **9c**), and aromatic fused ring (3-Indolyl **9d**, 3-benzothienyl **9e**), resulted in a dramatical decrease in the apoptosis activity (Fig. 7). These results are consistent with **8a** (Fig. 5A). Given the importance of the *para*-CF_3 group or the *meta*-CF_3 group, we introduced one $-CF_3$ group on the 3-pyridyl ring (**9f**). Consistently **9f** exhibited comparable activity to **B1071** (Fig. 7, Table S5). Together, the results indicated that a $-CF_3$ group that is properly positioned on a aryl ring is essential for the apoptotic activity.

The binding model of **BI1071** (Fig. 2B) showed that the N—H of one indole ring (indolyl 1, Fig. 2B) could form a hydrogen bond with the sidechain of His372. The importance of this hydrogen bond

Table 1
IC50 values of selected compounds against TNBC and colorectal cancer cells.

	Ar	R_1	X^-	IC_{50} (μM)					
				MDA-MB-231	BT549	MCF10A	HCT116	SW620	NCM460
8n	**4-CF_3-Ph**	**H**	**$MeSO_3$**	**0.22 ± 0.10**	**0.17 ± 0 .01**	**4.29 ± 0.09**	**0.27 ± 0.10**	**0.18 ± 0.02**	**6.84 ± 0.07**
8n-1	**4-CF_3-Ph**	**H**	**Cl**	**0.22 ± 0.09**	**0.17 ± 0.01**	**3.58 ± 0.14**	**0.26 ± 0.11**	**0.18 ± 0.02**	**5.13 ± 0.20**
8t	**3-CF_3-Ph**	**H**	**Cl**	**0.29 ± 0.10**	**0.07 ± 0.02**	**5.03 ± 0.09**	**0.31 ± 0.11**	**0.13 ± 0.02**	**10.0 ± 0.15**
9f	**6-CF_3-3-pyridyl**	**H**	**Cl**	**0.23 ± 0.11**	**0.05 ± 0.02**	**2.98 ± 0.16**	**0.35 ± 0.13**	**0.14 ± 0.02**	**8.10 ± 0.25**
10b	**4-CF_3-Ph**	**-Me**	**$MeSO_3$**	**0.06 ± 0.04**	**0.04 ± 0.02**	**2.19 ± 0.07**	**0.09 ± 0.05**	**0.10 ± 0.03**	**4.63 ± 0.20**
10c	**4-CF_3-Ph**	**-Et**	**Cl**	**0.08 ± 0.06**	**0.05 ± 0.02**	**1.50 ± 0.11**	**0.10 ± 0.07**	**0.10 ± 0.03**	**3.08 ± 0.13**
10d	**4-CF_3-Ph**	**-Pr**	**Cl**	**0.17 ± 0.10**	**0.10 ± 0.02**	**1.31 ± 0.16**	**0.35 ± 0.08**	**0.16 ± 0.02**	**5.09 ± 0.10**

IC_{50}: Concentration of the compound producing 50% cell growth inhibition after 24 h of drug exposure, as determined by the MTT assay. Data are presented as mean ± SD. Each experiment was performed at least 6 times. -Me: methyl, -Et: ethyl, -Pr: n-propyl.

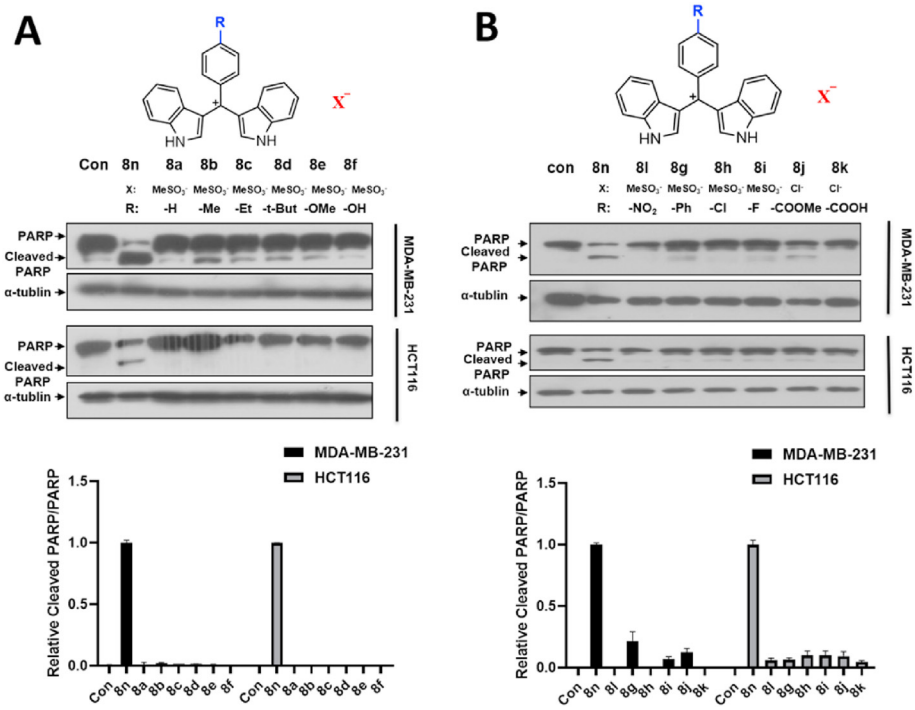

Fig. 5. Apoptotic activity of **BI1071** derivatives with different groups at the *para*-position of phenyl ring. MDA-MB-231 and HCT116 cells were treated with compounds (0.5 μM) for 6 h, and then cleaved PARP were analyzed by western blotting. The relative intensity ratio of PARP cleavage band/PARP band were counted and analyzed. (**A**) electron-donating groups as substitute at the *para*-position. (**B**) electron-withdrawing groups as substitute at the *para*-position. Data are presented as mean ± SD.

interaction was validated by **10a** (Fig. 8), in which replacing the H with $-CH_3$ on the N—H of both indole rings led to a sharp decrease in its apoptotic activity. The binding model of **BI1071** (Fig. 2B) also showed that the other indole ring (indolyl 2, Fig. 2B) bound to an open groove with limited contacts with the protein and lipophilic groups as substituents at the N—H of the indole ring could introduce additional hydrophobic interaction with the protein. Indeed, compound **10b** with a $-CH_3$ group at the N—H displayed much enhanced apoptotic activity compared to **8n** (Fig. 8, relative intensity ratio = 8.93 in MDA-MB-231 and 13.54 in HCT116, Table S6). Next, we explored the apoptotic effect of alkyl chains with different lengths at the N—H position of just one indole ring. Result exhibited that the apoptotic activity was gradually reduced when the length of alkyl chain was increased (**10b**, **10c**, **10d**, **10e** and **10f**) (Fig. 8). Modeling showed that the alkyl chain substituents at the N—H of indole ring 2 could enhance the interactions between the compound and the protein, however, steric hindrance would occur when the size of the alkyl chain increased, weakening the compound binding (Fig. 11).

The apoptotic effects of **8n(BI1071)** and **10b** were further tested in TNBC cell line BT549 and colorectal cancer cell line SW620 using PARP cleavage assay (Fig. 9A). **10b** showed stronger apoptotic activity than **8n**. The effects of **8n** and **10b** on cell death were further assessed using flow cytometry-based Annexin V/Propidium iodide (PI) apoptosis assay. Fig. 9B showed that about 65.53% of MDA-MB-231 cells were apoptotic when treated with 0.5 μM of **10b** for 6 h, while only 12.83% of cells were apoptotic in **8n**-treated cells. Similar results were observed in BT549 (**8n**-24.86%, **10b**-84.72%), HCT116 (**8n**-14.63%, **10b**-64.42%) and SW620 (**8n**-28.15%, **10b**-92.54%) cancer cells (Fig. 9B and C). Collectively, these data suggested that the pro-apoptotic effect of **10b** was stronger than **8n** in cancer cells.

4.2. In vitro anti-proliferative activity of the potent compounds

The potent compounds **8n(BI1071)**, **8n-1**, **8t**, **9f**, **10b**, **10c** and **10d** were further evaluated for their anticancer effect in both TNBC (MDA-MB-231 and BT 549) and colorectal (HCT116 and SW620) cancer cells using the 3-(4,5-dimethylthiazol-2-yl)-2,5-diphenyltetrazolium bromide (MTT) assay, and the IC_{50} values were listed in Table 1. Among these compounds, compounds **10b**

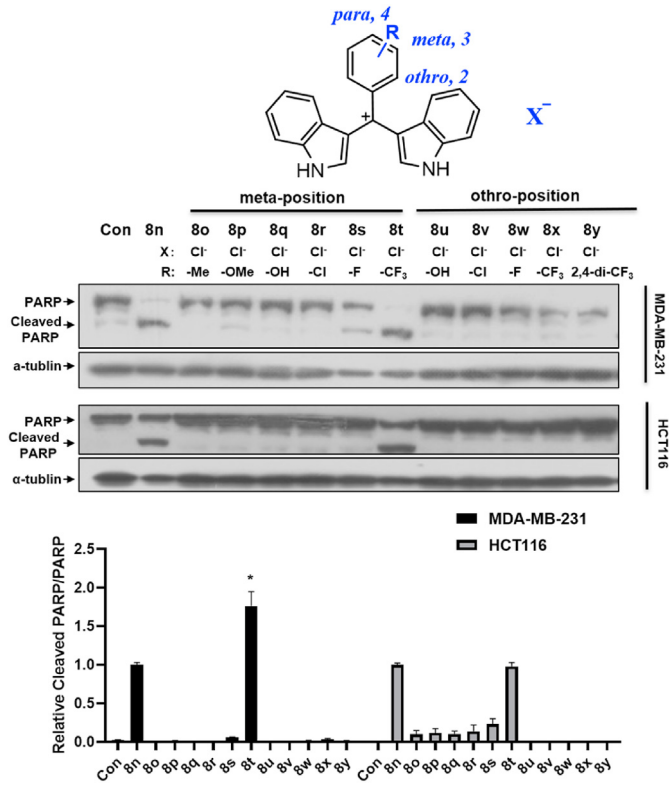

Fig. 6. Apoptotic activity of BI1071 derivatives with different groups at the *meta*- and *ortho*-position of phenyl ring. MDA-MB-231 and HCT116 cells were treated with compounds (0.5 μM) for 6 h, and then cleaved PARP were analyzed by western blotting. The relative intensity ratio of PARP cleavage band/PARP band were counted and analyzed. Data are presented as mean ± SD. $*p < 0.05$ compared to the 8n treated group (n = 3).

and **10c** displayed stronger anti-proliferative activity than **8n** in both of breast cancer cells (MDA-MB-231: 0.06 ± 0.04 μM for **10b** and 0.08 ± 0.06 μM for **10c**, BT549: 0.04 ± 0.02 μM for **10b** and 0.05 ± 0.02 μM for **10c**) and colorectal cancer cells (HCT116: 0.09 ± 0.05 μM for **10b** and 0.10 ± 0.07 μM for **10c**, SW620: 0.10 ± 0.03 μM for **10b** and 0.10 ± 0.03 μM for **10c**). We further used the non-cancerous breast epithelial cell line MCF10A and the non-transformed human colonic epithelial cell line NCM460 to test the compounds' selectivity against cancer cell lines. Compounds displayed good selectivity against cancer cells (Table 1). The most potent compound **10b** showed that the IC_{50} in normal mammary cells MCF10A was about 40-fold higher than in MDA-MB-231 and BT549, while in normal colon cells NCM460 was about 50-fold higher than in HCT116 and SW620.

4.3. Compounds' binding affinities to Nur77 protein

Next we evaluated the binding affinities of **10b** and **10c** to Nur77 protein. Fluorescence quenching assay and surface plasmon resonance (SPR) were utilized. The fluorescence emission spectra of Nur77-LBD (1 μM) in the presence of serial compound concentrations (0.01–1 μM) are shown in Fig. 10A. Interactions between the protein and compounds induced fluorescence quenching. The dissociation constant (K_d) of **BI1071** (**8n**) was measured as 217 nM (Fig. 10A). Compounds **10b** and **10c** bound to Nur77 with higher affinity than **8n** (K_d was 66 nM and 66 nM respectively, Fig. 10A). SPR was performed on BIAcore T200 instrument. Nur77-LBD was immobilized on a CM5 sensor chip, and gradient concentrations of compounds (0.01–5 μM) were injected into the flow cells in running buffer. The dissociation constant (K_d) of **8n**, **10b** and **10c** was measured as 110 nM, 33 nM and 36 nM, respectively (Fig. 10B). Taken together, results from the fluorescence quenching assay and the SPR methods consistently demonstrated that both **10b** and **10c** bind better to Nur77 than **8n.**

4.4. Molecular docking analysis

Compounds **10b** and **10c** displayed higher binding affinity to Nur77-LBD and improved anticancer activity, thus we perform molecular docking to further understand their binding mechanism. For **10b** and **10c**, the optimization strategy was to mimic the binding model of **BI1071** while introducing different alkyl groups at the N–H group on one of the indole rings to enhance compound's interaction with Nur77. The docking results showed that the binding models of **10b** and **10c** were almost identical to **BI1071** (Fig. 11). Indole ring 1 without alkyl substitution could establish a hydrogen bond with the polar residue of His372. Also, the phenyl ring could form *pi*-cation with Lys456. It is worth noting that the central carbonium of **10b** and **10c** other than the indolyl like **BI1071** could form additional *pi*-cation interaction with Try453. The $N–CH_3$ of **10b** and the $N–CH_2–CH_3$ of **10c** positioned closely to His494 to form good van der Waals interaction. The docking results may explain why compounds **10b** and **10c** exhibit slightly enhanced activity compared with **BI1071**.

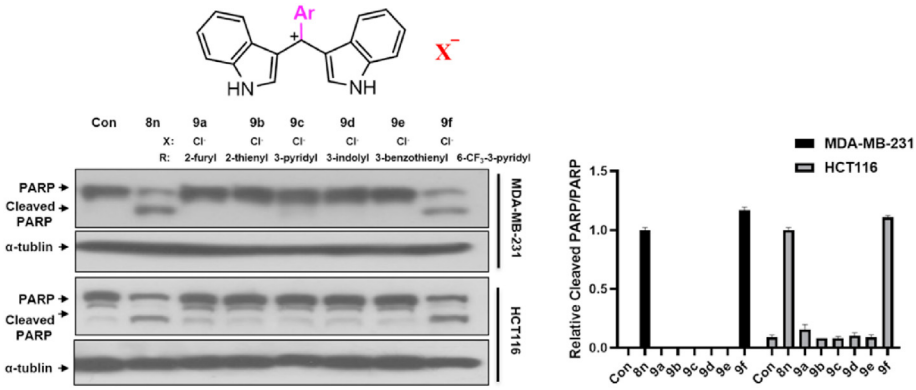

Fig. 7. Apoptotic activity of BI1071 with its phenyl ring replaced by different aromatic rings. MDA-MB-231 and HCT116 cells were treated with compounds (0.5 μM) for 6 h, and then cleaved PARP were analyzed by western blotting. The relative intensity ratio of PARP cleavage band/PARP band were counted and analyzed. Data are presented as mean ± SD.

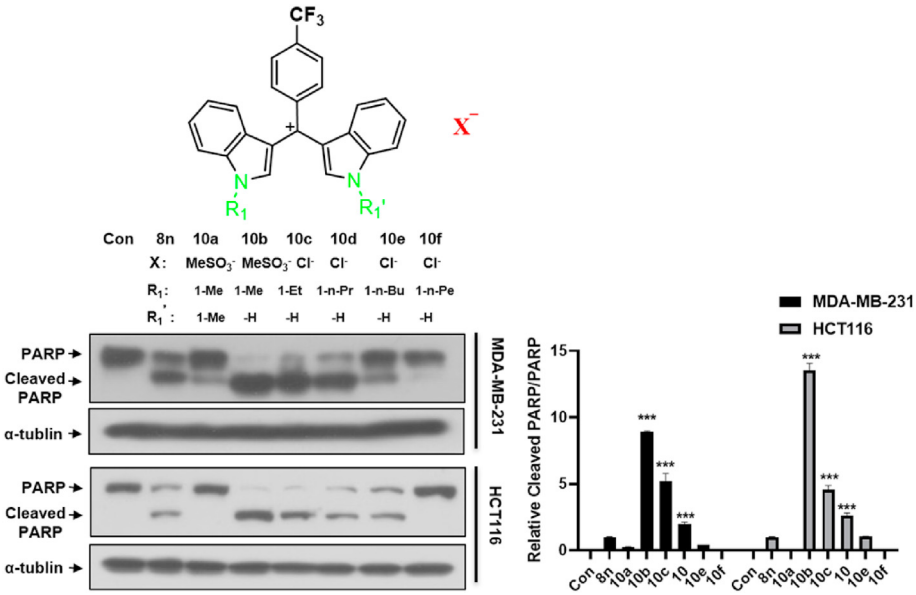

Fig. 8. Apoptotic activity of B1071 derivatives with substituents at the N—H of one indole ring. MDA-MB-231 and HCT116 cells were treated with compounds (0.5 μM) for 6 h, and then cleaved PARP were analyzed by western blotting. -Me: methyl, -Et: ethyl, -Pr: n-propyl, -Bu: n-butyl, -Pe: n-pentyl. The relative intensity ratio of PARP cleavage band/PARP band was counted and analyzed. Data are presented as mean ± SD. ***$p < 0.001$ compared to 8n treated group (n = 3).

4.5. *10b induces Nur77 mitochondrial targeting and its apoptotic effect is Nur77-dependent*

We next determined whether the strong apoptotic effect of **10b** is Nur77-dependent by examining its apoptotic activity in mouse embryonic fibroblast (MEF) and MEF lacking Nur77 (Nur77$^{-/-}$MEF). As expected **10b**, **10c**, **10d**, **and 9f** and could indeed induce the PARP cleavage in MEFs. However, such an apoptotic effect was significantly diminished in Nur77$^{-/-}$MEFs (Fig. 12A), implying that the apoptotic activities of these BI1071 analogs are Nur77-dependent. We showed previously that **8n** exerted its Nur77-dependent apoptotic effect by promoting Nur77 mitochondrial targeting [35]. Thus, we compared the effect of **10b** with **8n** on Nur77 mitochondrial targeting. HEK293T cells were transfected with Myc-Nur77 and subsequently treated with 0.5 μM **8n** or **10b**. Mitochondria-specific tracker using confocal microscopy revealed the localization of Myc-Nur77-LBD. The result showed that significantly more amount of transfected Myc-Nur77 accumulated in the mitochondria fraction when cells were treated with **10b** than with **8n** (Fig. 12C). The result was further confirmed by Western blotting (Fig. 12B). Taken together, these data demonstrated that compound **10b** exerted its Nur77-dependent apoptotic effect by inducing stronger Nur77 mitochondrial targeting than **8n**.

4.6. *Compound 10b promotes the interaction between Nur77 and Bcl-2 to induce Bcl-2 dependent apoptosis*

We have reported that **BI1071** (**8n**) induces apoptosis of cancer cells by activating the Nu77-Bcl-2 apoptotic pathway [35]. We therefore asked if derivatives of BI1071 utilize the same pathway to induce apoptosis by promoting the interactions between Nur77 and Bcl-2. The apoptotic effect of compounds **8n**, **10b**, **10c**, **10d**, **and 9f** was evaluated in MEFs and MEFs lacking Bcl-2 (Bcl-2$^{-/-}$MEF). At 0.5 μM, all test compounds effectively induced PARP cleavage in MEFs, while they had no apparent effect on PARP cleavage in Bcl-2$^{-/-}$MEFs (Fig. 13A). Then we determined if **10b** can induce Nur77 and Bcl-2 interaction. Cell-based Co-IP showed that Nur77 transfected in HEK293T cells interacted with Bcl-2 when cells were treated with **10b** (Fig. 13B). Moreover, confocal microscopy analysis revealed that **10b** promoted extensive mitochondrial colocalization of transfected GFP-Nur77 (Fig. 13C) or Myc-Nur77-LBD (Fig. 13D) with Bcl-2 in cells. Thus, binding of compound **10b** to Nur77 promotes Nur77 interaction with Bcl-2 and their mitochondrial colocalization.

4.7. *Antitumor effect of compound 10b in MMTV-PyMT-transgenic mouse models*

10b showed stronger apoptotic effect than **BI1071** *in vitro*. Therefore, its anticancer therapeutic potential was further investigated *in vivo*. MMTV-PyMT-transgenic mouse model was used for evaluating the *in vivo* efficacy of **10b** [35]. Administration of the MMTV-PyMT mice with **BI1071 (8n)** and **10b** (3 mg/kg) potently inhibited the growth of PyMT mammary tumor (Fig. 14A and B). **10b** possessed stronger *in vitro* apoptotic effect than **8n** in both of MDA-MB-231 and HCT116 cancer cells (Fig. 8 and Table 1). However, this difference was not directly translated in *in vivo* model. We found that the potency of **10b** was only slightly superior to **8n** (Fig. 14C), which could be attributed to their differences in ADME properties [46]. It is worthwhile noting that administration of **10b** did not show any apparent toxic effects such as loss of body weight (Fig. 14D).

4.8. *Pharmacokinetic (PK) study of compounds 10b and BI1071 in rats*

To gain some insight into why **10b**'s superiority to **BI1071**(**8n**) *in vitro* did not translate *in vivo*, we carried out pharmacokinetic (PK) study of compounds **10b** and **BI1071 (8n)** in Sprague-Dawley (SD) rats. Compounds were administered by oral absorption (PO, 5 mg/kg) or intravenous injection (IV, 0.5 mg/kg). It is worth noting that **8n** displays more favorable pharmacokinetic properties in female rat than male rat (Table S7). As shown in Table 2, **8n** has a better oral bioavailability in female rats (F = 22.79%) than in male rats (F = 20.12%), and possesses a higher maximal plasma concentration as well in female rats (C_{max} = 203.25 ± 17.15 μg/L in female and C_{max} = 143.37 ± 20.05 μg/L in male). In addition, the

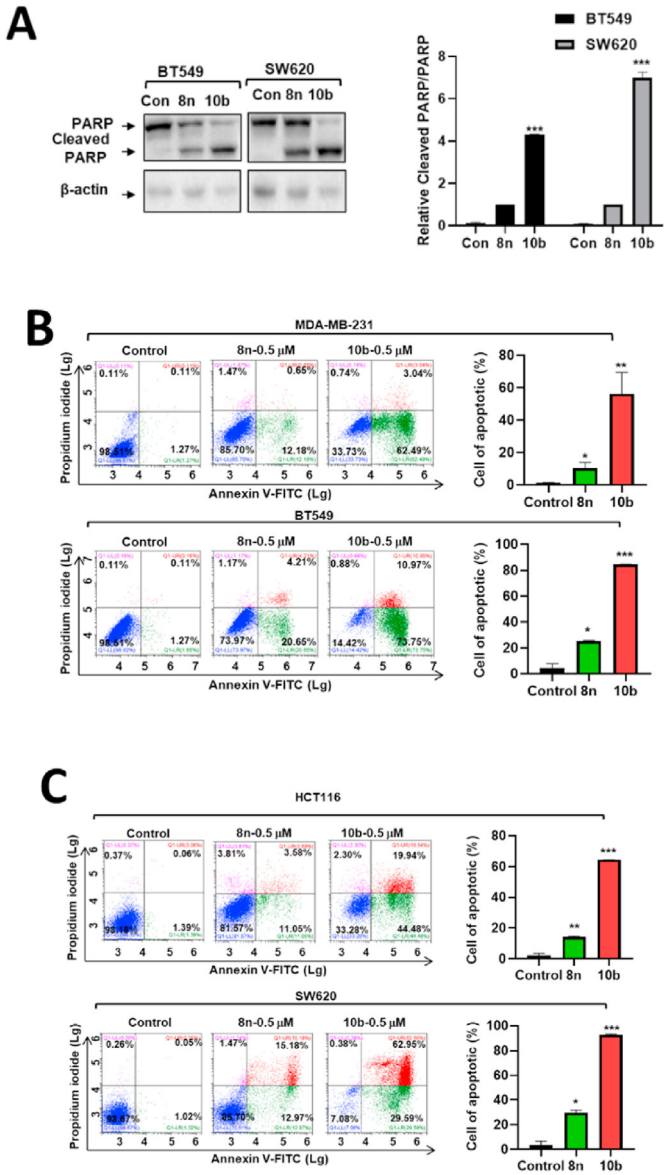

Fig. 9. Apoptotic activity of **8n(BI1071)** and **10b** in TNBC and colorectal cancer cells. (**A**) BT549 and SW620 cells were treated with 0.5 μM **8n** and **10b** respectively for 6 h, and then cleaved PARP were analyzed by western blotting. Data are presented as mean ± SD. ***$p < 0.001$ compared to 8n treated group (n = 3). (**B**–**C**) Annexin V/PI staining of MDA-MB-231, BT549, HCT116 and SW620 cells treated with 0.5 μM **8n** and **10b** respectively for 6 h was analyzed by flow cytometry. Data are presented as mean ± SD. *$p < 0.05$, **$p < 0.01$, ***$p < 0.001$ compared to control group (n = 3).

time of maximum concentration (T_{max} = 5.33 ± 2.31 h) was the same for both the male and female rats, but the elimination half-life and the mean residence times in female rats ($T_{1/2}$ = 6.81 ± 4.35 h, MRT = 14.50 ± 0.78 h) are slight longer than male rats ($T_{1/2}$ = 5.28 ± 2.91 h, MRT = 12.32 ± 1.06 h). It is interesting to note that **10b** displayed less gender differences between male and female rats (Table S8). However, compound **10b** reveals poorer PK profile in rats compared to compound **8n** with a low AUC, short half-life, and low bioavailability (Table 2). The low bioavailability may be the reason why compound **10b** did not display significantly better antitumor activity *in vivo* than **8n**, although it had a much stronger apoptotic effect *in vivo* than **8n**.

Detected by LC/MS/MS, liquid chromatography/tandem mass spectrometry. AUC, area under the concentration–time curve. C_{max}, maximum plasma concentration. T_{max}, the time of maximum concentration. $T_{1/2}$, elimination half-life. MRT, mean residence time. CL, total plasma clearance. V_{ss}, apparent volume of the plasma compartment. F, oral bioavailability. PO, per oral. IV, intravenous. a, the number of rats is 3. b, the number of rats is 4, 2 male and 2 female rats.

5. Conclusion

Compound **BI1071** (**8n**) is a novel modulator of Nur77. In this study we carried out some preliminary optimization work of **BI1071** using the structure-based design approach. 36 **BI1071** derivatives were synthesized and evaluated for their apoptosis activities. Analyses of the structure activity relationship (SAR) indicated that: a): A $-CF_3$ group at the *meta*- or *para*-position of phenyl ring is essential for maintaining the outstanding apoptosis activity. b): The *ortho*-substituent on the phenyl ring goes against its activity. c): The activity of the asymmetric mono-alkyl substitution on the N–H of one indole moiety is better than the symmetric *di*-alkyl substitution, and the alkyl chain with 1–3 carbons is the most favorable moiety. Among the 36 derivatives, compound **10b** showed the most potent activity at molecular, cellular and animal levels. **10b** could bind to target protein Nur77 with higher affinity and strongly activate the Nur77-Bcl-2 apoptotic pathway. The PK profiling in rats reflected that **10b** displayed a suitable drug exposure (AUC) and half-life ($T_{1/2}$), but a low bioavailability. Hence, compound **10b** has been selected as a lead candidate and is currently undergoing further optimization in our follow-up studies.

6. Experimental section

6.1. Chemistry

All the materials were obtained from commercial suppliers and used without purification, unless otherwise specified. ^{1}H NMR (600 MHz) and ^{13}C NMR (150 MHz) spectra were performed on Bruker spectrometers (Bruker in Asia Pacific, Beijing, China) in DMSO-d_6 or CD_3OD with TMS as the internal reference. The values of chemical shifts are expressed in ppm. MS spectra were taken in ESI mode on Q-Exactive apparatus (ThermoFisher, Shanghai, China). Column chromatography was performed on Biotage (Prime). The purity of all tested compounds was detected by HPLC performed on waters e2695 instrument.

6.1.1. General procedure for the synthesis of symmetric Ph-C-DIM (*3a – 3y, 4a - 4f, 5a*)

Indole (50.0 g, 0.427 mol, 2 equiv) and *p*-trifluoromethylbenzaldehyde (37.1 g, 0.214 mol, 1 equiv) and CH_3OH (200 mL) were added to the round-bottom flask (500 mL). Then 37% HCl(2.34 g, 0.0214 mol, 0.1 equiv) was diluted in water (19 mL, ten-fold dilution), the aqueous was slowly added to round-bottom flask. The mixture was stirred at room temperature, and monitored by TLC until the reaction was completed. The solution was neutralized by 5% NaOH to pH = 7. The solvent methanol was evaporated under reduced pressure to give oily liquid mixed with water. The resident was extracted with ethyl acetate (50 mL * 3). The EA phase was combined and dried over anhydrous Na_2SO_4. The organic solvent was evaporated to obtain a crude product which was purified by recrystallization (CH_3OH/H_2O), *p*-CF_3-Ph-C-DIM yielded as a white powder (80.2 g, 96.4%)

3a – 3y, **4a - 4f**, and **5a** (0.1–1 mmol) were synthesized according this general method, the crude products were purified by silica-gel column chromatography (Ethyl acetate/Hexane).

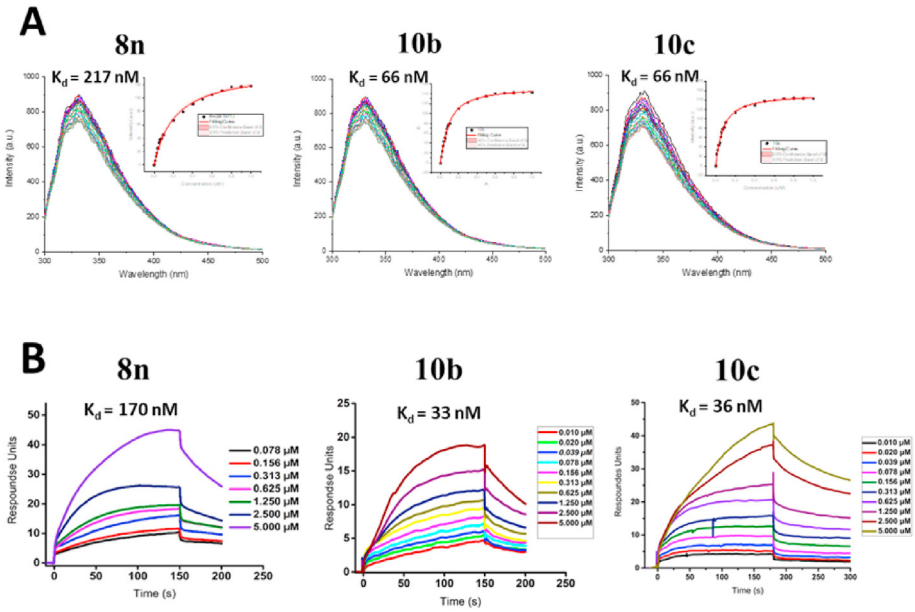

Fig. 10. Nur77 binding affinity of **10b** and **10c**. (**A**) fluorescence quenching assay, 1 μM Nur77-LBD was titrated by successive additions of a 0.01–1 μM compound solution. The excitation wavelength was 280 nm, and the emission measurement range was 300–500 nm. The maximum fluorescence intensities at 330 nm with increasing concentrations of compound were selected for curve fitting. (**B**) surface plasmon resonance (SPR) assay. Nur77-LBD was immobilized on a CM5 sensor chip, and gradient concentrations of compounds (0.01–5 μM) were injected into the flow cells in running buffer at a flow rate of 30 μL/min for a 150-s association phase followed by a 420-s dissociation phase and a 30-s regeneration phase.

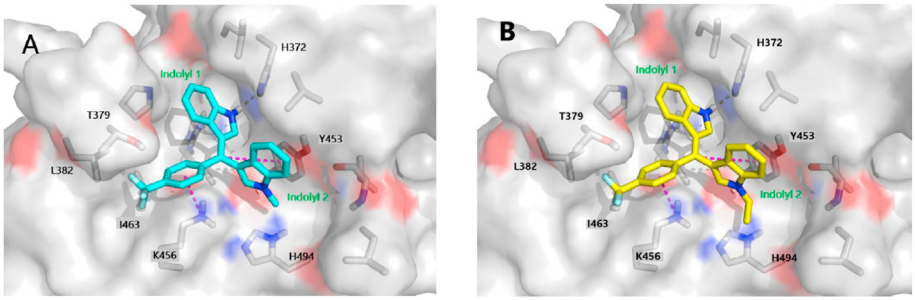

Fig. 11. Proposed binding model for **10b** (cyan stick, **A**) and **10c** (yellow stick, **B**) in site B of Nur77-LBD (PDB: 3V3Q). The protein was represented as surface mode, the hydrophobic residues were colored in gray, and the polar residues were decorated with blue and red, respectively. The H-bonds and *pi*-cation were shown in yellow dashed lines and magenta dashed lines, respectively. (For interpretation of the references to color in this figure legend, the reader is referred to the Web version of this article.)

*6.1.2. General procedure for the synthesis of asymmetric Ph-C-DIM (**7a - 7f**)*

Indole (1.17 g, 10 mmol, 3 equiv), 4-(trifluoromethyl)benzaldehyde (0.58 g, 3.3 mmol, 1 equiv), and tetramethyl guanidine (TMG, 76 mg, 0.66 mmol, 0.2 equiv) were added to a round bottom flask (100 mL). Pure water (50 mL) was added to the flask, and the reaction was stirred vigorously at room temperature for 24 h. The reaction mixture was extracted with ethyl acetate (50 mL * 3). The organic phase was collected, dried over anhydrous Na_2SO_4 and purified by silica-gel column chromatography (Ethyl acetate/Hexane), to give a white product (1H-3-indolyl)(4-CF_3-phenyl)methanol (**6a**, 623 mg, yield: 65%).

6a (1 mmol, 1 equiv) and alkyl-N-indole **1b** - **1f** (1.5 mmol, 1.5 equiv) were added to 25 mL sealed tube equipped with trifluoroethanol (5 mL). The reaction was stirred at 50 °C for 4 h, and the solvent was evaporated under reduced pressure. The final crude product was purified by silica-gel column chromatography (Ethyl acetate/Hexane) to give white compound **7a** - **7f**.

*6.1.3. General procedure for the synthesis of Ph-C-DIM$^+$ (**8a - 8y**, **9a - 9f**, and **10a - 10f**)*

The synthesis procedure of Ph-C-DIM$^+$MeSO$_3^-$ (**8a** - **8i**, **8l** - **8n** and **10a** - **10b**).

Ph-C-DIM (1 equiv), pyridinium dichromate (1.4 equiv) and $MeSO_3H$ (10 equiv) were added to a flask containing methanol. The mixture was stirred at room temperature for 1 h. Then, the methanol was evaporated under reduced pressure to obtain a mixture. The mixture was dissolved with 1-butanol and washed with water. The organic layer was evaporated under reduced pressure to obtain a crude product. Finally, the crude product was purified by silica-gel column chromatography (CH_2Cl_2/MeOH/$MeSO_3H$) to afford Ph-C-DIM$^+$MeSO$_3^-$.

The synthesis procedure of Ph-C-DIM$^+$Cl$^-$ (**8a-1**, **8f-1**, **8j** - **8k**, **8n-1**, **8o** - **8y**, **9a** - **9f** and **10c** - **10f**).

Ph-C-DIM (1 equiv), pyridinium dichromate (1.4 equiv) and HCl (37%, 10 equiv) were added to a flask containing methanol. The mixture was stirred at room temperature for 1 h. Then, the

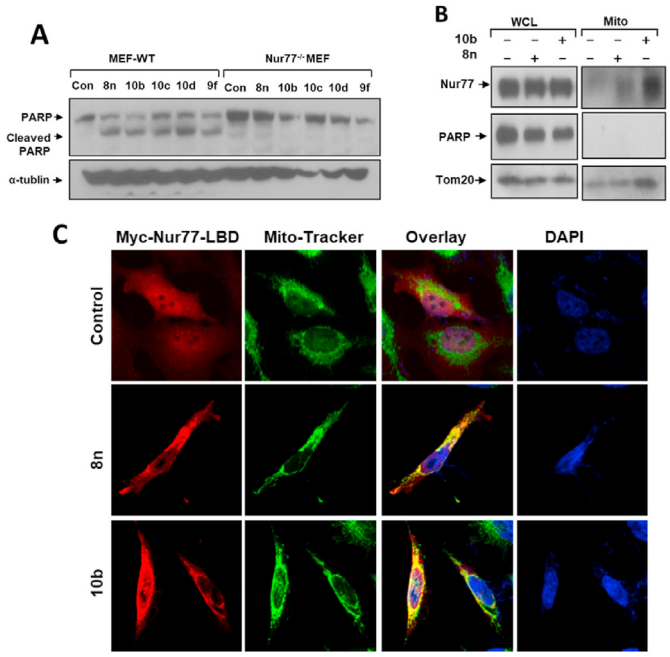

Fig. 12. 10b induced Nur77-dependent apoptosis and Nur77 mitochondrial targeting. (**A**) PARP cleavage in MEFs or Nur77$^{-/-}$MEFs treated with 0.5 μM potent compounds as showed for 6 h was determined by Western blotting. (**B**). HEK293T cells were transfected with Myc-Nur77. Whole cell lysate (WCL) and mitochondria fractions (Mito) were prepared from HEK293T cells treated with 0.5 μM **8n** and **10b** respectively for 2 h, and analyzed by Western blotting. Expression of nuclear PARP and mitochondrial Tom20 was shown to ensure the purity of mitochondrial fraction. (**C**). HEK293T cells transfected with Myc-Nur77-LBD were treated with **8n** and **10b** (0.5 μM) respectively for 2 h were immunestained with Mito-Tracker (Green) and visualized by confocal microscopy. (For interpretation of the references to color in this figure legend, the reader is referred to the Web version of this article.)

methanol was evaporated under reduced pressure to obtain a mixture. The mixture was dissolved with 1-butanol and washed with saturated NaCl solution. The organic layer was evaporated under reduced pressure to obtain a crude product. Finally, the crude product was purified by silica-gel column chromatography (CH_2Cl_2/MeOH/HCl) to afford Ph-C-DIM$^+$Cl$^-$.

6.1.4. Di(1H-indol-3-yl)(phenyl)methylium methanesulfonate (8a)

Compound **8a** was obtained according to **general procedure 6.1.3.** 0.310 mmol Ph-C-DIM was used. Compound **8a** was obtained as red solid (94 mg, yield = 73%). HPLC purity: 99.85%. ^{1}H NMR (600 MHz, DMSO-d_6) 14.02 (br. s., 2H, 1-indole-H), 8.68 (br. s., 2H, 2-indole-H), 7.84–7.98 (m, 1H, 4-Ar-H), 7.63–7.79 (m, 6H, 4-indole-H, 2,3,5,6-Ar-H), 7.39 (t, J = 7.61 Hz, 2H, 6-indole-H), 7.15 (t, J = 7.52 Hz, 2H, 5-indole-H), 6.67 (br. s., 2H, 7-indole-H), 2.37 (s, 3H, $-SO_3CH_3$). ^{13}C NMR (151 MHz, DMSO-d_6) 169.7(C$^+$, 1C), 147.8 (2C), 140.3 (2C), 136.7 (1C), 133.9 (2C), 133.0 (1C),129.9 (2C), 127.2 (2C), 126.2 (2C), 124.7 (2C), 121.8 (2C), 121.5 (2C), 115.0 (2C). HRMS (ESI) calcd for $C_{23}H_{17}N_2^+$[M]$^+$: 321.1386, found: 321.1385.

6.1.5. Di(1H-indol-3-yl)(phenyl)methylium chloride (8a-1)

Compound **8a-1** was obtained according to **general procedure 6.1.3.** 0.310 mmol Ph-C-DIM was used. Compound **8a-1** was obtained as red solid (85 mg, yield = 77%). HPLC purity >98%. ^{1}H NMR (600 MHz, DMSO-d_6) 14.44 (br. s., 2H, 1-indole-H), 8.68 (br. s., 2H, 2-indole-H), 7.88 (td, J = 7.29, 1.38 Hz, 1H, 4-Ar-H), 7.74 (d, J = 8.07 Hz, 2H, 4-indole-H), 7.65–7.72 (m, 4H, 2,3,5,6-Ar-H), 7.38 (t, J = 7.61 Hz, 2H, 6-indole-H), 7.12 (t, J = 7.51 Hz, 2H, 5-indole-H), 6.66 (br. s., 2H, 7-indole-H). ^{13}C NMR (151 MHz, DMSO-d_6) 169.3 (C$^+$, 1C), 147.3 (2C), 139.8 (2C), 137.8 (1C), 133.5 (2C), 132.3 (1C), 129.4 (2C), 126.7 (2C), 125.7 (2C), 124.2 (2C), 121.3 (2C), 121.0 (2C), 114.5 (2C). HRMS (ESI, m/z) calcd for $C_{23}H_{17}N_2^+$[M]$^+$: 321.1386, found: 321.1385.

6.1.6. Di(1H-indol-3-yl)(p-tolyl)methylium methanesulfonate (8b)

Compound **8b** was obtained according to **general procedure 6.1.3.** 0.15 mmol Ph-C-DIM was used. Compound **8b** was obtained as red solid (52 mg, yield = 81%). HPLC purity >98%. ^{1}H NMR (600 MHz, DMSO-d_6) 13.95 (br. s., 2H, 1-indole-H), 8.60 (br. s., 2H, 2-indole-H), 7.72 (d, J = 0 8.07 Hz, 2H, 2,6-Ar-H), 7.59 (d, J = 7.70 Hz, 2H, 4-indole-H), 7.52 (d, J = 7.70 Hz, 2H, 3,5-Ar-H), 7.39 (t, J = 7.61 Hz, 2H, 6-indole-H), 7.16 (t, J = 7.52 Hz, 2H, 5-indole-H), 6.77 (d, J = 6.97 Hz, 2H, 7-indole-H), 2.55 (s, 3H, $-CH_3$), 2.35 (s, 3H, $-SO_3CH_3$). ^{13}C NMR (151 MHz, DMSO-d_6) 169.3(C$^+$, 1C), 147.2 (2C), 144.7 (2C), 139.7 (2C), 133.1 (1C), 130.0 (2C), 126.7 (2C), 125.7 (3C), 124.2 (2C), 121.4 (2C), 121.1 (2C), 114.5 (2C), 39.1 (1C), 21.4 (1C). HRMS (ESI) calcd for $C_{24}H_{19}N_2^+$[M]$^+$: 335.1543, found: 335.1541.

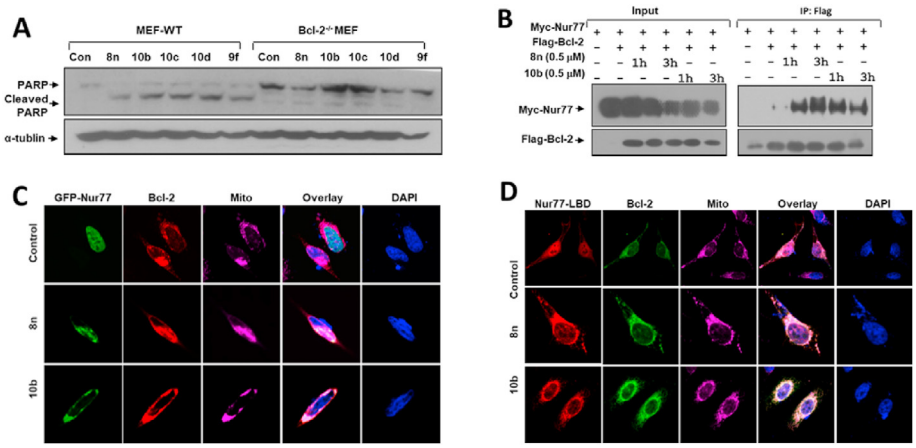

Fig. 13. 10b induced Bcl-2 dependent apoptosis by promoting the interaction between Nur77 and Bcl-2. (**A**) PARP cleavage in MEFs or Bcl-2$^{-/-}$MEFs treated with 0.5 μM potent compounds as showed for 6 h was determined by Western blotting. (**B**) HEK293T transfected with Flag-Bcl-2 together with Myc-Nur77 were treated with or without 0.5 μM **8n** and **10b** respectively for indicated time and analyzed by co-immunoprecipitation assays using anti-Flag antibody. (**C-D**) Co-localization of Nur77 with Bcl-2. HEK293T cells were transfected with Flag-Bcl-2 together with GFP-Nur77 (**C**) or GFP-Nur77-LBD (**D**), treated with or without 0.5 μM **8n** and **10b** respectively for 2 h, stained with anti-flag antibody, and visualized using confocal microscopy.

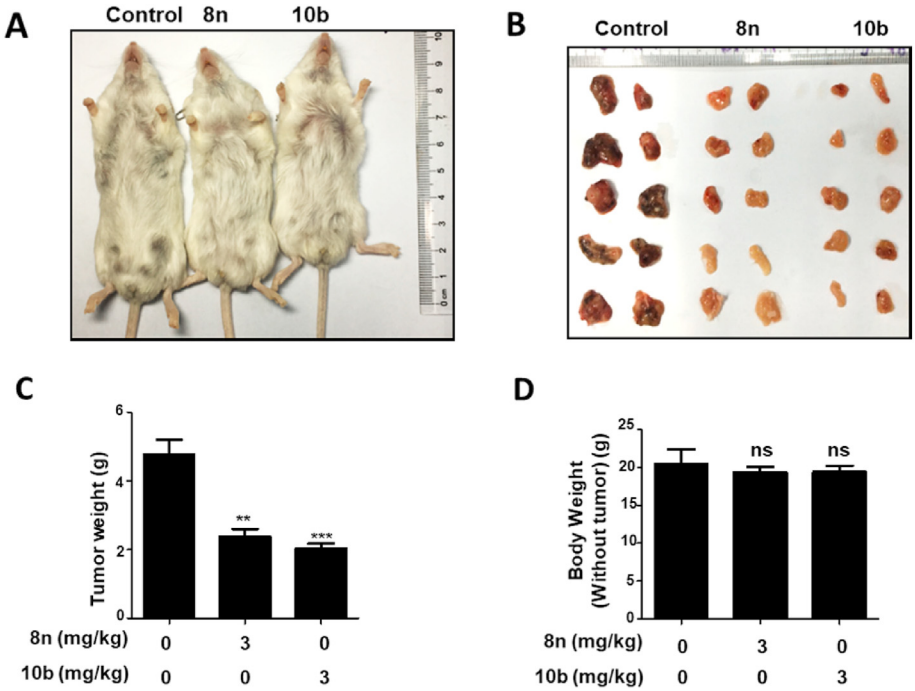

Fig. 14. Antitumor effect of compound **10b** in MMTV-PyMT-transgenic mouse models. (**A-B**) Representative images of MMTV—PyMT mammary tumor model mice and tumors from mice administered with or without **8n** and **10b** respectively. For MMTV-PyMT mammary tumor model, female wild-type MMTV-PyMT mice of 12 weeks old were randomly divided into two groups (n = 6), treated daily with an oral dose of 3 mg/kg **8n** and **10b** respectively for 14 days. (**C**) Inhibition of PyMT tumor growth by **8n** and **10b**. Mice treated with **8n** and **10b** respectively, and tumors were weighted (n = 6). Data are presented as mean ± SD. $^{**}p < 0.01$, $^{***}p < 0.001$ compared to control group (n = 6) (**D**) 14 days after administration of **8n** and **10b** respectively, MMTV-PyMT mice without tumor were weighted. Data are presented as mean ± SD, ns, no significant difference.

Table 2
Pharmacokinetic parameters of compound **10b** and **BI1071** in rats. Data are presented as mean ± SD.

Compound	Route		$AUC_{0\text{-}t}$ (μg/L*h)	C_{max} (μg/L)	T_{max} (h)	$T_{1/2}$ (h)	$MRT_{0\text{-}t}$ (h)	CL (L/h/kg)	V_{ss} (L/kg)	F (%)
BI1071 (8n)	IV(0.5 mg/kg)	Male[a]	1116.00 ± 136.33	879.60 ± 123.02		4.05 ± 0.91	4.31 ± 0.86	0.45 ± 0.05	2.56 ± 0.27	
		female[a]	1731.98 ± 69.97	1636.90 ± 191.04		5.91 ± 1.48	3.59 ± 0.32	0.28 ± 0.01	2.38 ± 0.53	
	PO(5 mg/kg)	Male[a]	2245.71 ± 491.07	143.37 ± 20.05	5.33 ± 1.16	5.28 ± 2.91	12.32 ± 1.06			20.12
		female[a]	3947.28 ± 97.00	203.25 ± 17.15	5.33 ± 2.31	6.81 ± 4.35	14.50 ± 0.78			22.79
10b	IV(0.5 mg/kg)	Male/female[b]	501.35 ± 72.71	560.79 ± 91.56		2.66 ± 0.30	0.56 ± 0.68	1.02 ± 0.17	3.69 ± 0.63	
	PO(5 mg/kg)	Male/female[b]	733.56 ± 138.08	57.93 ± 9.15	3 ± 0	4.49 ± 1.93	9.59 ± 1.44			14.63

6.1.7. (4-ethylphenyl)di(1H-indol-3-yl)methylium methanesulfonate (8c)

Compound **8c** was obtained according to **general procedure 6.1.3.** 0.57 mmol Ph-C-DIM was used. Compound **8c** was obtained as red solid (172 mg, yield = 68%). HPLC purity >98%. ^{1}H NMR (600 MHz, DMSO-d_6) 13.93 (br. s., 2H, 1-indole-H), 8.60 (br. s., 2H, 2-indole-H), 7.72 (d, J = 8.07 Hz, 2H, 2,6-Ar-H), 7.62 (d, J = 7.89 Hz, 2H, 3,5-Ar-H), 7.55 (d, J = 8.07 Hz, 2H, 4-indole-H), 7.40 (t, J = 7.61 Hz, 2H, 6-indole-H), 7.16 (t, J = 7.61 Hz, 2H, 5-indole-H), 6.76 (br. s., 2H, 7-indole-H), 2.85 (q, J = 7.64 Hz, 2H, $-CH_2$-), 2.35 (s, 3H, $-SO_3CH_3$), 1.33 (t, J = 7.61 Hz, 3H, $-CH_3$). ^{13}C NMR (151 MHz, METHANOL-d_4) 172.5 (1C, C^+), 153.5 (2C), 147.5 (2C), 141.3 (2C), 135.6 (1C), 130.2 (2C), 128.2 (2C), 127.4 (3C), 125.8 (2C), 123.7 (2C), 123.1 (2C), 115.3 (2C), 39.6 (1C), 30.2 (1C), 15.8 (1C). HRMS (ESI) calcd for $C_{25}H_{21}N_2^+[M]^+$: 349.1699, found: 349.1701.

6.1.8. (4-(tert-butyl)phenyl)di(1H-indol-3-yl)methylium methanesulfonate (8d)

Compound **8d** was obtained according to **general procedure 6.1.3.** 0.53 mmol Ph-C-DIM was used. Compound **8d** was obtained as red solid (202 mg, yield = 81%). HPLC purity >98%. ^{1}H NMR (600 MHz, DMSO-d_6) 13.91 (br. s., 2H, 1-indole-H), 8.57 (br. s., 2H, 2-indole-H), 7.73 (m, 4H, 2,6-Ar-H, 4-indole-H), 7.62 (d, J = 8.25 Hz, 2H, 3,5-Ar-H), 7.40 (t, J = 7.61 Hz, 2H, 6-indole-H), 7.16 (t, J = 7.61 Hz, 2H, 5-indole-H), 6.74 (br. s., 2H, 7-indole-H), 2.37 (s, 3H, $-SO_3CH_3$), 1.43 (s, 9H, $-CH_3$). ^{13}C NMR (151 MHz, DMSO-d_6) 169.7 (1C, C^+), 158.0 (2C), 147.6 (2C), 140.0 (2C), 133.8 (1C), 126.6 (4C), 126.2 (3C), 124.7 (2C), 121.8 (2C), 121.6 (2C), 115.0 (2C), 35.6 (1C), 31.4 (3C). HRMS(ESI) calcd for $C_{27}H_{25}N_2^+[M]^+$: 377.2012, found: 377.2013.

6.1.9. Di(1H-indol-3-yl)(4-methoxyphenyl)methylium methanesulfonate (8e)

Compound **8e** was obtained according to **general procedure 6.1.3.** 0.16 mmol Ph-C-DIM was used. Compound **8e** was obtained as red solid (62 mg, yield = 87%). HPLC purity >98%.^{1}H NMR (600 MHz, DMSO-d_6) 13.83 (br. s., 2H, 1-indole-H), 8.56 (br. s., 2H, 2-indole-H), 7.72 (d, J = 8.07 Hz, 2H, 2,6-Ar-H), 7.69 (d, J = 7.89 Hz, 2H, 3,5-Ar-H), 7.40 (t, J = 7.61 Hz, 2H, 6-indole-H), 7.26 (d, J = 8.62 Hz, 2H, 4-indole-H), 7.17 (t, J = 7.61 Hz, 2H, 5-indole-H), 6.86 (br. s., 2H, 7-indole-H), 3.98 (s, 3H, $-OCH_3$), 2.36 (s, 3H, $-SO_3CH_3$). ^{13}C NMR (151 MHz, DMSO-d_6) 168.9 (1C, C^+), 164.7 (1C, $-OCH_3$-C), 146.7 (2C), 139.5 (2C), 129.1 (1C), 126.2 (4C), 124.1 (2C), 121.1 (4C), 115.0 (2C), 114.3 (4C), 56.0 (1C, $-OCH_3$). HRMS (ESI) calcd for $C_{24}H_{19}N_2O^+[M]^+$: 351.1492, found: 351.1488.

6.1.10. (4-hydroxyphenyl)di(1H-indol-3-yl)methylium methanesulfonate (8f)

Compound **8f** was obtained according to **general procedure 6.1.3.** 0.30 mmol Ph-C-DIM was used. Compound **8f** was obtained as red solid (73 mg, yield = 56%). HPLC purity: 97%.^{1}H NMR (600 MHz, DMSO-d_6) 13.73 (br. s., 2H, 1-indole-H), 11.12 (br. s., 1H, −OH), 8.50 (br. s., 2H, 2-indole-H), 7.71 (d, J = 8.07 Hz, 2H, 2,6-Ar-H), 7.59 (d, J = 7.34 Hz, 2H, 3,5-Ar-H), 7.39 (t, J = 7.70 Hz, 2H, 6-indole-H), 7.17 (t, J = 7.43 Hz, 2H, 5-indole-H), 7.07 (d, J = 8.62 Hz, 2H, 4-indole-H), 6.90 (br. s., 2H, 7-indole-H), 2.35 (s, 3H, $-SO_3CH$). ^{13}C NMR (151 MHz, DMSO-d_6) 169.5 (1C, C$^+$), 164.4 (1C, -C-OH), 146.2 (2C), 139.4 (2C), 127.3 (1C), 125.5 (2C), 123.9 (2C), 121.0 (4C), 116.6 (4C), 114.2 (4C). HRMS (ESI) calcd for $C_{23}H_{17}N_2O^+[M]^+$: 337.1335, found: 337.1332.

6.1.11. (4-hydroxyphenyl)di(1H-indol-3-yl)methylium chloride (8f-1)

Compound **8f-1** was obtained according to **general procedure 6.1.3.** 1.48 mmol Ph-C-DIM was used. Compound **8f-1** was obtained as red solid (314 mg, yield = 57%). HPLC purity: 96%. ^{1}H NMR (600 MHz, DMSO-d_6) 13.86 (br. s., 2H, 1-indole-H), 11.20 (br. s., 1H, −OH), 8.50 (br. s., 2H, 2-indole-H), 7.71 (d, J = 8.07 Hz, 2H, 2,6-Ar-H), 7.59 (d, J = 7.34 Hz, 2H, 3,5-Ar-H), 7.39 (t, J = 7.70 Hz, 2H, 6-indole-H), 7.17 (t, J = 7.43 Hz, 2H, 5-indole-H), 7.09 (d, J = 8.62 Hz, 2H, 4-indole-H), 6.91 (br. s., 2H, 7-indole-H). ^{13}C NMR (151 MHz, DMSO-d_6) 169.6 (1C, C$^+$), 164.4 (1C, -C-OH), 146.0 (2C), 139.4 (2C), 127.3 (1C), 125.4 (2C), 123.9 (2C), 120.9 (4C), 116.6 (4C), 114.2 (4C). HRMS (ESI) calcd for $C_{23}H_{17}N_2O^+[M]^+$: 337.1335, found: 337.1331.

6.1.12. [1,1′-biphenyl]-4-yldi(1H-indol-3-yl)methylium methanesulfonate (8g)

Compound **8g** was obtained according to **general procedure 6.1.3.** 0.50 mmol Ph-C-DIM was used. Compound **8g** was obtained as red solid (216 mg, yield = 88%). HPLC purity >98%.^{1}H NMR (600 MHz, DMSO-d_6) 13.98 (br. s., 2H, 1-indole-H), 8.67 (br. s., 2H, 2-indole-H), 8.06 (d, J = 8.25 Hz, 2H, 3,5-Ar-H), 7.93 (d, J = 7.34 Hz, 2H, 2,6-Ar-H), 7.79 (d, J = 7.89 Hz, 2H, 2′,6′-Ar-H), 7.74 (d, J = 8.07 Hz, 2H, 4-indole-H), 7.58 (t, J = 7.70 Hz, 2H, 3′,5′-Ar-H), 7.48−7.53 (m, 1H, 4′-Ar-H), 7.41 (t, J = 7.61 Hz, 2H, 6-indole-H), 7.18 (t, J = 7.61 Hz, 2H, 5-indole-H), 6.83 (br. s., 2H, 7-indole-H), 2.35 (s, 3H, $-SO_3CH_3$). ^{13}C NMR (151 MHz, DMSO-d_6) 168.21 (1C, C$^+$), 147.9 (2C), 145.5 (1C), 140.1 (2C), 138.8 (2C), 134.9 (1C), 129.8 (2C), 129.4 (2C), 127.8 (2C), 127.6 (4C), 126.3 (2C), 124.5 (2C), 121.9 (2C), 121.7 (2C), 115.0 (2C). HRMS (ESI) calcd for $C_{29}H_{21}N_2^+[M]^+$: 397.1699, found: 397.1703.

6.1.13. (4-chlorophenyl)di(1H-indol-3-yl)methylium methanesulfonate (8h)

Compound **8h** was obtained according to **general procedure 6.1.3.** 0.75 mmol Ph-C-DIM was used. Compound **8h** was obtained as red solid (239 mg, yield = 71%). HPLC purity >98%. ^{1}H NMR (600 MHz, DMSO-d_6) 13.92 (br. s, 2H, 1-indole-H) 8.65 (br. s., 2H, 2-indole-H) 7.78 (d, J = 8.25 Hz, 2H, 3,5-Ar-H) 7.68−7.75 (m, 4H, 2,6-Ar-H, 4-indole-H) 7.41 (t, J = 7.61 Hz, 2H, 6-indole-H) 7.19 (t, J = 7.52 Hz, 2H, 5-indole-H) 6.76 (d, J = 6.79 Hz, 2H, 7-indole-H) 2.35 (br. s, 3H, $-SO_3CH_3$). ^{13}C NMR (151 MHz, DMSO-d_6) 167.47 (1C, C$^+$), 148.27 (2C), 140.38 (2C), 139.11 (2C), 134.97 (1C), 130.03 (2C), 126.88 (2C), 126.39 (2C), 124.92 (3C), 121.96 (2C), 121.66 (2C), 115.08 (2C). HRMS (ESI) calcd for $C_{23}H_{16}ClN_2^+[M]^+$: 355.0997, found: 355.0991.

6.1.14. (4-fluorophenyl)di(1H-indol-3-yl)methylium methanesulfonate (8i)

Compound **8i** was obtained according to **general procedure 6.1.3.** 0.57 mmol Ph-C-DIM was used. Compound **8i** was obtained as red solid (198 mg, yield = 80%). HPLC purity: 97%. ^{1}H NMR (600 MHz, DMSO-d_6) 13.99 (br. s., 2H, 1-indole-H), 8.65 (br. s., 2H, 2-indole-H), 7.77 (d, J = 8.34 Hz, 2H, 3,5-Ar-H), 7.72 (d, J = 8.07 Hz, 2H, 2,6-Ar-H), 7.55 (t, J = 8.71 Hz, 2H, 4-indole-H), 7.40 (t, J = 7.61 Hz, 2H, 6-indole-H), 7.18 (t, J = 7.61 Hz, 2H, 5-indole-H), 6.76 (br. s., 2H, 7-indole-H), 2.34 (s, 3H, $-SO_3CH_3$). ^{13}C NMR (151 MHz, DMSO-d_6) 167.8 (1C, C$^+$), 165.55 (d, J = 257.49 Hz, 1C, -C-F), 147.7 (2C), 139.8 (2C), 135.5 (1C), 126.6 (2C), 125.9 (4C), 124.4 (2C), 121.5 (2C), 121.2 (2C), 116.74 (d, J = 20.91 Hz, 2C, -C-C-F), 114.5 (2C). HRMS (ESI) calcd for $C_{23}H_{16}FN_2^+[M]^+$: 339.1292, found: 339.1296.

6.1.15. Di(1H-indol-3-yl)(4-(methoxycarbonyl)phenyl)methylium chloride (8j)

Compound **8j** was obtained according to **general procedure 6.1.3.** 0.30 mmol Ph-C-DIM was used. Compound **8j** was obtained as red solid (110 mg, yield = 89%). HPLC purity >98%. ^{1}H NMR (600 MHz, DMSO-d_6) 14.40 (br. s., 2H, 1-indole-H), 8.72 (br. s., 2H, 2-indole-H), 8.22 (d, J = 7.34 Hz, 2H, 4-indole-H), 7.82 (d, J = 7.15 Hz, 2H, 3,5-Ar-H), 7.72 (d, J = 7.34 Hz, 2H, 2,6-Ar-H), 7.38 (br. s., 2H, 6-indole-H), 7.19 (br. s., 2H, 5-indole-H), 6.62 (br. s., 2H, 7-indole-H), 3.96 (s, 3H, $-CH_3$). ^{13}C NMR (151 MHz, DMSO-d_6) 167.6 (1C, C$^+$), 166.1 (1C, −C═O), 148.3 (2C), 140.4 (2C), 133.6 (2C), 133.0 (1C), 130.4 (2C), 126.9 (2C), 126.4 (3C), 125.0 (2C), 121.9 (2C), 121.6 (2C), 115.1 (2C), 53.2 (1C). HRMS (ESI) calcd for $C_{25}H_{19}N_2O_2^+[M]^+$: 379.1441, found: 379.1434.

6.1.16. Bis(1H-indol-3-yl)(4-carboxyphenyl)methylium chloride (8k)

Compound **8k** was obtained according to **general procedure 6.1.3** (acetone was used as solvent). 0.30 mmol Ph-C-DIM was used. Compound **8k** was obtained as red solid (67 mg, yield = 56%). HPLC purity >98%. ^{1}H NMR (600 MHz, DMSO-d_6) 14.21 (br. s, 2H, 1-indole-H), 13.56 (br. s., 1H, −COOH), 8.67 (br. s., 2H, 2-indole-H), 8.20 (d, J = 8.25 Hz, 2H, 4-indole-H), 7.79 (d, J = 8.07 Hz, 2H, 3,5-Ar-H), 7.71 (d, J = 8.07 Hz, 2H, 2,6-Ar-H), 7.39 (t, J = 7.61 Hz, 2H, 6-indole-H), 7.15 (t, J = 7.61 Hz, 2H, 5-indole-H), 6.66 (br. s., 2H, 7-indole-H). ^{13}C NMR (151 MHz, DMSO-d_6) 172.0 (1C, C$^+$), 167.2 (1C, −C═O), 148.2 (2C), 142.3 (1C), 140.8 (2C), 134.8 (2C), 132.8 (1C), 130.5 (2C), 127.0 (2C), 126.3 (2C), 124.8 (2C), 122.0 (2C), 121.6 (2C), 115.2 (2C). HRMS (ESI) calcd for $C_{24}H_{17}N_2O_2^+[M]^+$: 365.1285, found: 365.1272.

6.1.17. Di(1H-indol-3-yl)(4-nitrophenyl)methylium methanesulfonate (8l)

Compound **8l** was obtained according to **general procedure 6.1.3.** 0.54 mmol Ph-C-DIM was used. Compound **8l** was obtained as red solid (184 mg, yield = 74%). HPLC purity >98%. ^{1}H NMR (600 MHz, DMSO-d_6) 14.14 (br. s., 2H, 1-indole-H), 8.75 (br. s., 2H, 2-indole-H), 8.50 (d, J = 8.44 Hz, 2H, 4-indole-H), 7.97 (d, J = 8.44 Hz, 2H, 3,5-Ar-H), 7.73 (d, J = 8.07 Hz, 2H, 2,6-Ar-H), 7.42 (t, J = 7.61 Hz, 2H, 6-indole-H), 7.17 (t, J = 7.52 Hz, 2H, 5-indole-H), 6.70 (br. s., 2H, 7-indole-H), 2.35 (s, 3H, $-SO_3CH_3$). ^{13}C NMR (151 MHz, DMSO-d_6) 165.6 (1C, C$^+$), 150.0 (2C), 148.4 (2C), 145.1 (1C), 139.9 (2C), 133.4 (1C), 126.2 (4C), 124.7 (2C), 124.4 (2C), 121.6 (2C), 121.4 (2C), 114.7 (2C). HRMS (ESI) calcd for $C_{23}H_{16}N_3O_2^+[M]^+$: 366.1241, found: 366.1241.

6.1.18. Di(1H-indol-3-yl)(4-(trifluoromethyl)phenyl) methylium methanesulfonate (8n)

Compound **8n** was obtained according to **general procedure 6.1.3.** 0.26 mmol Ph-C-DIM was used. Compound **8n** was obtained as red solid (104 mg, yield = 83%). HPLC purity >98%.^{1}H NMR (600 MHz, DMSO-d_6) 14.06 (br. s., 2H, 1-indole-H), 8.71 (br. s., 2H, 2-indole-H), 8.07 (d, J = 8.07 Hz, 2H, 3,5-Ar-H), 7.91 (d, J = 7.70 Hz, 2H, 2,6-Ar-H), 7.73 (d, J = 8.07 Hz, 2H, 4-indole-H), 7.42 (t, J = 7.61 Hz,

2H, 6-indole-H), 7.19 (t, J = 7.52 Hz, 2H, 5-indole-H), 6.67 (br. s., 2H, 7-indole-H), 2.33 (br. s., 3H, $-SO_3CH_3$). ^{13}C NMR (151 MHz, DMSO-d_6) 166.6 (1C, C^+), 148.3 (2C), 139.9 (2C), 133.2 (1C), 132.4 (q, J_{C-F} = 29.7 Hz, 1C, 4-Ar-C), 126.2 (6C), 126.1 (2C), 124.6 (2C), 124.0 (q, J_{C-F} = 274.0 Hz, 1C, $-CF_3$), 121.6 (2C), 121.3 (2C), 114.7 (2C). HRMS (ESI) calcd for $C_{24}H_{16}F_3N_2^+[M]^+$: 389.1260, found: 389.1255.

6.1.19. Di(1H-indol-3-yl)(4-(trifluoromethyl)phenyl) methylium chloride (8n-1)

Compound **8n-1** was obtained according to **general procedure 6.1.3.** 0.26 mmol Ph-C-DIM was used. Compound **8n-1** was obtained as red solid (93 mg, yield = 85%). HPLC purity >98%.^1H NMR (600 MHz, DMSO-d_6) 14.48 (br. s., 2H, 1-indole-H), 8.69 (br. s., 2H, 2-indole-H), 8.05 (br. s., 2H, 3,5-Ar-H), 7.89 (br. s., 2H, 2,6-Ar-H), 7.74 (br. s., 2H, 4-indole-H), 7.40 (br. s., 2H, 6-indole-H), 7.17 (br. s., 2H, 5-indole-H), 6.64 (br. s., 2H, 7-indole-H). ^{13}C NMR (151 MHz, DMSO-d_6) 166.3 (1C, C^+), 148.0 (2C), 140.0 (2C), 133.1 (1C), 132.4 (q, J_{C-F} = 29.7 Hz, 1C, 4-Ar-C), 126.2 (6C), 126.0 (2C), 124.6 (2C), 124.0 (q, J_{C-F} = 274.0 Hz, 1C, $-CF_3$), 121.6 (2C), 121.2 (2C), 114.7 (2C). HRMS (ESI, *m/z*) calcd for $C_{24}H_{16}F_3N_2^+[M]^+$: 389.1260, found: 389.1255.

6.1.20. Di(1H-indol-3-yl)(m-tolyl)methylium chloride (8o)

Compound **8o** was obtained according to **general procedure 6.1.3.** 0.60 mmol Ph-C-DIM was used. Compound **8o** was obtained as red solid (189 mg, yield = 85%). HPLC purity: 97%.^1H NMR (600 MHz, DMSO-d_6) 14.11 (br. s, 2H, 1-indole-H) 8.60 (br. s., 2H, 2-indole-H) 7.71 (d, J = 7.70 Hz, 2H, 4-indole-H) 7.68 (d, J = 6.97 Hz, 1H, 6-Ar-H) 7.58 (t, J = 7.15 Hz, 1H, 5-Ar-H) 7.48 (s, 1H, 2-Ar-H) 7.44 (d, J = 6.97 Hz, 1H,4-Ar-H) 7.37 (t, J = 7.06 Hz, 2H, 6-indole-H) 7.13 (t, J = 7.24 Hz, 2H, 5-indole-H) 6.69 (d, J = 5.69 Hz, 2H, 7-indole-H) 2.39 (s, 3H, $-CH_3$). ^{13}C NMR (151 MHz, DMSO-d_6) 168.9 (1C, C^+), 147.2 (2C), 140.0 (2C), 138.8 (1C), 134.1 (2C), 129.6 (1C), 129.3 (1C), 126.7 (1C), 125.7 (3C), 124.2 (3C), 121.5 (2C), 121.1 (2C), 114.6 (2C), 20.8 (1C). HRMS (ESI) calcd for $C_{24}H_{19}N_2^+[M]^+$: 335.1543, found: 335.1540.

6.1.21. Di(1H-indol-3-yl)(3-methoxyphenyl)methylium chloride (8p)

Compound **8p** was obtained according to **general procedure 6.1.3.** 0.57 mmol Ph-C-DIM was used. Compound **8p** was obtained as red solid (167 mg, yield = 76%). HPLC purity >98%.^1H NMR (600 MHz, DMSO-d_6) 14.08 (br. s., 2H, 1-indole-H), 8.62 (br. s., 2H, 2-indole-H), 7.71 (d, J = 7.70 Hz, 2H, 4-indole-H), 7.60 (br. s., 1H, 5-Ar-H), 7.43 (d, J = 7.15 Hz, 1H, 6-Ar-H), 7.37 (t, J = 7.24 Hz, 2H, 6-indole-H), 7.21 (d, J = 7.15 Hz, 1H, 4-Ar-H), 7.18 (br. s., 1H, 2-Ar-H), 7.14 (t, J = 7.34 Hz, 2H, 5-indole-H), 6.72 (d, J = 7.15 Hz, 2H, 7-indole-H), 3.76 (s, 3H, $-OCH_3$). ^{13}C NMR (151 MHz, DMSO-d_6) 168.1 (1C, C^+), 159.6 (1C, -C-OCH_3), 147.4 (2C), 140.1 (2C), 139.3 (1C), 130.6 (2C), 126.7 (1C), 125.8 (2C), 124.3 (2C), 121.5 (2C), 121.2 (2C), 119.1 (2C), 117.1 (1C), 114.6 (2C), 55.6 (1C). HRMS (ESI) calcd for $C_{24}H_{19}N_2O^+[M]^+$: 351.1492, found: 351.1489.

6.1.22. (3-hydroxyphenyl)di(1H-indol-3-yl)methylium chloride (8q)

Compound **8q** was obtained according to **general procedure 6.1.3.** 0.70 mmol Ph-C-DIM was used. Compound **8q** was obtained as red solid (170 mg, yield = 65%). HPLC purity >98%. ^1H NMR (400 MHz, DMSO-d_6) 14.28 (br. s., 2H, 1-indole-H), 10.17 (br. s., 1H, $-OH$), 8.65 (br. s., 2H, 2-indole-H), 7.73 (br. s., 2H, 4-indole-H), 7.50 (br. s., 1H, 5-Ar-H), 7.39 (br. s., 2H, 6-indole-H), 7.30 (br. s., 1H, 6-Ar-H), 7.17 (br. s., 2H, 5-indole-H), 7.07 (br. s., 1H, 4-Ar-H), 7.04 (br. s., 1H, 2-Ar-H), 6.77 (br. s., 2H, 7-indole-H). ^{13}C NMR (151 MHz, DMSO-d_6) 169.4 (1C, C^+), 158.0 (1C, -C-OH), 147.2 (1C), 139.7 (2C), 139.1 (1C), 130.5 (2C), 126.7 (1C), 125.7 (2C), 124.3 (2C), 122.8 (1C), 121.3 (2C) 121.2 (2C), 120.5 (2C), 128.3 (1C), 114.3 (2C). HRMS (ESI) calcd for $C_{23}H_{17}N_2O^+[M]^+$: 337.1335, found: 337.1331.

6.1.23. (3-chlorophenyl)di(1H-indol-3-yl)methylium chloride (8r)

Compound **8r** was obtained according to **general procedure 6.1.3.** 0.25 mmol Ph-C-DIM was used. Compound **8r** was obtained as red solid (90 mg, yield = 92%). HPLC purity >98%. ^1H NMR (400 MHz, DMSO-d_6) 14.47 (br. s., 2H, 1-indole-H), 8.93 (br. s., 2H, 2-indole-H), 7.83 (br. s., 2H, 4-indole-H), 7.55–7.75 (m, 4H), 7.37 (br. s., 2H, 6-indole-H), 7.14 (br. s., 2H, 5-indole-H), 6.45 (br. s., 2H, 7-indole-H). ^{13}C NMR (151 MHz, DMSO-d_6) 164.2 (1C, C^+), 148.3 (2C), 141.6 (2C), 134.4 (1C), 132.9 (1C), 131.7 (2C), 131.2 (1C), 127.1 (1C), 126.2 (2C), 124.6 (2C), 124.6 (2C), 122.2 (2C), 121.5 (2C), 114.9 (2C). HRMS (ESI) calcd for $C_{23}H_{16}ClN_2\ ^+[M]^+$: 355.0997, found: 355.0990.

6.1.24. (3-fluorophenyl)di(1H-indol-3-yl)methylium chloride (8s)

Compound **8s** was obtained according to **general procedure 6.1.3.** 0.21 mmol Ph-C-DIM was used. Compound **8s** was obtained as red solid (71 mg, yield = 91%). HPLC purity >98%. ^1H NMR (600 MHz, DMSO-d_6) 14.42 (br. s., 2H, 1-indole-H), 8.72 (br. s., 2H, 2-indole-H), 7.74 (m, 4H), 7.58 (d, J = 8.80 Hz, 1H, 4-Ar-H), 7.52 (d, J = 5.69 Hz, 1H, 6-Ar-H), 7.40 (t, J = 6.60 Hz, 2H, 6-indole-H), 7.18 (t, J = 6.60 Hz, 2H, 5-indole-H), 6.68 (br. s., 2H, 7-Ar-H). ^{13}C NMR (151 MHz, METHANOL-d_4) 170.0 (1C, C^+), 164.3 (d, J_{C-F} = 247.59 Hz, 1C, 3-F-Ar-C), 148.1 (2C), 141.2 (2C), 132.6 (2C), 127.8 (2C), 127.6 (4C), 126.0 (2C), 123.4 (2C), 122.9 (2C), 122.5 (d, J_{C-F} = 20.9 Hz, 1C, Ar–C), 115.6 (2C). HRMS (ESI, *m/z*) calcd for $C_{23}H_{16}FN_2\ ^+[M]^+$: 339.1292, found: 339.1288.

6.1.25. Di(1H-indol-3-yl)(3-(trifluoromethyl)phenyl)methylium chloride (8t)

Compound **8t** was obtained according to **general procedure 6.1.3.** 0.427 mmol Ph-C-DIM was used. Compound **8t** was obtained as red solid (161 mg, yield = 89%). HPLC purity >98%. ^1H NMR (600 MHz, DMSO-d_6) 14.62 (br. s., 2H, 1-indole-H), 8.70 (br. s., 2H, 2-indole-H), 8.22 (d, J = 7.89 Hz, 1H, 4-Ar-H), 8.02 (s, 1H, 2-Ar-H), 7.96–8.00 (m, 1H, 6-Ar-H), 7.91–7.95 (m, 1H, 5-Ar-H), 7.76 (d, J = 8.25 Hz, 2H, 4-indole-H), 7.39 (t, J = 7.61 Hz, 2H, 6-indole-H), 7.15 (t, J = 7.61 Hz, 2H, 5-indole-H), 6.62 (d, J = 5.69 Hz, 2H, 7-indole-H). ^{13}C NMR (151 MHz, DMSO-d_6) 166.2 (1C, C^+), 148.4 (2C), 140.7 (2C), 139.3 (1C), 136.7 (1C), 131.1 (q, J_{C-F} = 3.3 Hz, 1C, Ar–C), 130.5 (q, J_{C-F} = 31.9 Hz, 1C, 3-Ar-C), 129.9 (q, J_{C-F} = 3.3 Hz, 1C, Ar–C), 129.2 (1C), 126.9 (2C), 126.3 (2C), 124.8 (2C), 124.3 (q, J_{C-F} = 272.9 Hz, 1C, $-CF_3$), 122.0 (2C), 121.4 (2C), 115.3 (2C). HRMS (ESI, *m/z*) calcd for $C_{24}H_{16}F_3N_2^+[M]^+$: 389.1260, found: 389.1264.

6.1.26. (2-hydroxyphenyl)di(1H-indol-3-yl)methylium chloride (8u)

Compound **8u** was obtained according to **general procedure 6.1.3.** 0.75 mmol Ph-C-DIM was used. Compound **8u** was obtained as red solid (156 mg, yield = 56%). HPLC purity: 96%. ^1H NMR (600 MHz, DMSO-d_6) 14.10 (br. s., 2H, 1-indole-H), 10.36 (br. s., 1H, $-OH$), 8.71 (br. s., 2H, 2-indole-H), 7.68 (d, J = 8.07 Hz, 2H, 4-indole-H), 7.60–7.66 (m, 1H, -H-Ar), 7.36 (t, J = 7.61 Hz, 1H, 4-Ar-H), 7.26–7.30 (m, 1H,-H-Ar), 7.20 (d, J = 8.25 Hz, 1H, 3-Ar-H), 7.15 (t, J = 7.70 Hz, 2H, 6-indole-H), 7.04 (t, J = 7.52 Hz, 2H, 5-indole-H), 6.79 (d, J = 6.05 Hz, 2H, 7-indole-H). ^{13}C NMR (151 MHz, DMSO-d_6) 166.9 (1C, C^+), 156.6 (1C, -C-OH), 146.5 (2C), 139.5 (2C), 134.5 (2C), 132.5 (1C), 127.0 (1C), 125.5 (2C), 124.6 (1C), 124.2 (2C), 122.0 (1C), 120.6 (2C), 119.9 (2C), 117.0 (1C), 114.2 (2C). HRMS (ESI) calcd for $C_{23}H_{17}N_2O^+[M]^+$: 337.1335, found: 337.1330.

6.1.27. (2-chlorophenyl)di(1H-indol-3-yl)methylium chloride (8v)

Compound **8v** was obtained according to **general procedure 6.1.3.** 0.27 mmol Ph-C-DIM was used. Compound **8v** was obtained as red solid (84 mg, yield = 79%). HPLC purity >98%. ^1H NMR (600 MHz, DMSO-d_6) 14.59 (br. s., 2H, 1-indole-H), 8.94 (br. s., 2H, 2-

indole-H), 7.84 (br. s., 2H, 4-indole-H), 7.73 (m, 2H, Ar—H), 7.67 (br. s., 1H, Ar—H), 7.61 (br. s., 1H, Ar—H), 7.37 (br. s., 2H, 6-indole-H), 7.14 (br. s., 2H, 5-indole-H), 6.46 (br. s., 2H, 7-indole-H). ^{13}C NMR (151 MHz, DMSO-d_6) 164.1 (1C, C$^+$), 147.4 (2C), 139.6 (2C), 136.2 (1C), 133.3 (1C), 131.8 (1C), 131.5 (1C), 130.8 (1C), 128.5 (1C), 126.2 (2C), 125.8 (2C), 124.7 (2C), 121.0 (2C), 120.2 (2C), 114.5 (2C). HRMS (ESI, *m/z*) calcd for $C_{23}H_{16}ClN_2^+$[M]$^+$: 355.0997, found: 355.0992.

6.1.28. (2-fluorophenyl)di(1H-indol-3-yl)methylium chloride (8w)

Compound **8w** was obtained according to **general procedure 6.1.3.** 0.27 mmol Ph-C-DIM was used. Compound **8w** was obtained as red solid (57 mg, yield = 56%). HPLC purity >98%. ^{1}H NMR (600 MHz, DMSO-d_6) 14.48 (br. s., 2H, 1-indole-H), 8.82 (br. s., 2H, 2-indole-H), 7.90 (br. s., 1H, -H-Ar), 7.72 (br. s., 2H, 4-indole-H), 7.62 (br. s., 1H, -H-Ar), 7.50—7.58 (m, 2H, -H-Ar), 7.38 (br. s., 2H, 6-indole-H), 7.15 (br. s., 2H, 5-indole-H), 6.64 (br. s., 2H, 7-indole-H). ^{13}C NMR (151 MHz, DMSO-d_6) 160.6 (1C, C$^+$), 159.43 (d, J = 251.99 Hz, 1C, -C-F), 147.5 (2C), 140.0 (2C), 135.25 (d, J = 7.70 Hz, 1C, -C-C-C-F), 133.0 (1C), 126.5 (2C), 125.9 (3C), 125.2 (1C), 124.6 (2C), 121.6 (2C), 120.3 (2C), 116.98 (d, J = 22.01 Hz, 1C, -C-C-F), 114.7 (2C). HRMS (ESI) calcd for $C_{23}H_{16}FN_2^+$[M]$^+$: 339.1292, found: 339.1292.

6.1.29. Di(1H-indol-3-yl)(2-(trifluoromethyl)phenyl)methylium chloride (8x)

Compound **8x** was obtained according to **general procedure 6.1.3.** 0.26 mmol Ph-C-DIM was used. Compound **8x** was obtained as red solid (101 mg, yield = 93%). HPLC purity >98%.^{1}H NMR (600 MHz, DMSO-d_6) 14.63 (br. s., 2H, 1-indole-H), 8.94 (br. s., 2H, 2-indole-H), 8.11 (m, 1H, 3-Ar-H), 7.99 (br. s., 2H, 4-indole-H), 7.68 (m, 3H, Ar—H), 7.31 (br. s., 2H, 6-indole-H), 7.08 (br. s., 2H, 5-indole-H), 6.22 (br. s., 2H, 7-indole-H). ^{13}C NMR (151 MHz, DMSO-d_6) 164.4 (1C, C$^+$), 147.0 (2C), 139.0 (2C), 136.0 (1C), 133.4 (q, $J_{C\text{-}F}$ = 3.3 Hz, 1C, Ar—C), 131.6 (1C), 130.2 (q, $J_{C\text{-}F}$ = 3.3 Hz, 1C, Ar—C), 127.3 (1C), 126.3 (q, $J_{C\text{-}F}$ = 33.0 Hz, 1C, 2-Ar-C), 125.8 (2C), 125.4 (2C), 124.3 (2C), 122.8 (q, $J_{C\text{-}F}$ = 274.0 Hz, 1C, —CF_3), 120.5 (2C), 119.9 (2C), 114.2 (2C). HRMS (ESI, *m/z*) calcd for $C_{24}H_{16}F_3N_2^+$ [M]$^+$: 389.1260, found: 389.1262.

6.1.30. (2,4-bis(trifluoromethyl)phenyl)di(1H-indol-3-yl)methylium chloride (8y)

Compound **8y** was obtained according to **general procedure 6.1.3.** 0.25 mmol Ph-C-DIM was used. Compound **8y** was obtained as red solid (116 mg, yield = 94%). HPLC purity: 98%. ^{1}H NMR (600 MHz, DMSO-d_6) 14.55 (br. s., 2H, 1-indole-H), 8.91 (br. s., 2H, 2-indole-H), 8.48 (br. s., 1H, 3-Ar-H), 8.40 (d, J = 6.60 Hz, 1H, 5-Ar-H), 7.99 (d, J = 6.60 Hz, 1H, 6-Ar-H), 7.71 (d, J = 7.15 Hz, 2H, 4-indole-H), 7.38 (br. s., 2H, 6-indole-H), 7.16 (br. s., 2H, 5-indole-H), 6.38 (br. s., 2H, 7-indole-H). ^{13}C NMR (151 MHz, DMSO-d_6) 162.5 (1C, C$^+$), 148.8 (2C), 141.2 (1C), 140.5 (2C), 133.1 (q, $J_{C\text{-}F}$ = 3.3 Hz, 1C, Ar—C), 132.40 (q, $J_{C\text{-}F}$ = 31.9 Hz, 1C, Ar—C), 131.2 (1C), 129.1 (q, $J_{C\text{-}F}$ = 34.1 Hz, 1C, Ar—C), 126.6 (2C), 126.5 (2C), 125.6 (2C), 125.4 (1C), 123.6 (q, $J_{C\text{-}F}$ = 272.9 Hz, 1C, Ar—C), 123.2 (q, $J_{C\text{-}F}$ = 275.1 Hz, 1C, Ar—C), 121.7 (2C), 121.2 (2C), 115.4 (2C). HRMS (ESI, *m/z*) calcd for $C_{25}H_{15}F_6N_2^+$ [M]$^+$: 457.1134, found: 457.1135.

6.1.31. Furan-2-yldi(1H-indol-3-yl)methylium chloride (9a)

Compound **9a** was obtained according to **general procedure 6.1.3.** 0.64 mmol Ph-C-DIM was used. Compound **9a** was obtained as red solid (196 mg, yield = 88%). HPLC purity: 98%. ^{1}H NMR (600 MHz, DMSO-d_6) 14.19 (br. s., 2H, 1-indole-H), 8.66 (s, 2H, 2-indole-H), 8.60 (s, 1H, Ar—H), 7.71—7.81 (m, 3H), 7.40 (t, J = 7.43 Hz, 2H, 6-indole-H), 7.15—7.23 (m, 3H), 6.94 (d, J = 7.15 Hz, 2H, 7-indole-H). ^{13}C NMR (151 MHz, METHANOL-d$_4$) 153.9 (1C, C$^+$), 152.5 (1C), 151.1 (1C), 144.7 (2C), 139.2 (2C), 129.7 (1C), 126.0 (2C), 125.7 (2C), 124.1 (2C), 121.7 (2C), 118.0 (2C), 115.7 (1C), 113.8 (2C). HRMS (ESI, *m/z*) calcd for $C_{21}H_{15}N_2O^+$[M]$^+$: 311.1179, found: 311.1170.

6.1.32. Di(1H-indol-3-yl)(thiophen-2-yl)methylium chloride (9b)

Compound **9b** was obtained according to **general procedure 6.1.3.** 1.00 mmol Ph-C-DIM was used. Compound **9b** was obtained as red solid (270 mg, yield = 75%). HPLC purity >98%.^{1}H NMR (600 MHz, DMSO-d_6) 14.24 (br. s., 2H, 1-indole-H), 8.64 (d, J = 4.22 Hz, 1H, 4-Ar-H), 8.62 (s, 2H, 2-indole-H), 8.00 (d, J = 2.57 Hz, 1H, 2-Ar-H), 7.76 (d, J = 8.07 Hz, 2H, 4-indole-H), 7.64 (t, J = 3.85 Hz, 1H, 3-Ar-H), 7.40 (t, J = 7.61 Hz, 2H, 6-indole-H), 7.14 (t, J = 7.52 Hz, 2H, 5-indole-H), 6.85 (d, J = 7.15 Hz, 2H, 7-indole-H). ^{13}C NMR (151 MHz, METHANOL-d$_4$) 159.4 (1C, C$^+$), 145.1 (2C), 143.0 (1C), 141.4 (1C), 139.8 (1C), 139.3 (2C), 130.6 (1C), 125.9 (4C), 124.1 (2C), 121.8 (2C), 121.0 (2C), 113.8 (2C). HRMS (ESI, *m/z*) calcd for $C_{21}H_{15}N_2S^+$[M]$^+$: 327.0950, found: 327.0955.

6.1.33. Di(1H-indol-3-yl)(pyridin-3-yl)methylium chloride (9c)

Compound **9c** was obtained according to **general procedure 6.1.3.** 0.62 mmol Ph-C-DIM was used. Compound **9c** was obtained as red solid (147 mg, yield = 67%). HPLC purity >98%. ^{1}H NMR (600 MHz, DMSO-d_6) 14.55 (br. s., 2H, 1-indole-H), 9.07 (br. s., 1H, 2-Ar-H), 8.89 (br. s., 1H, 6-Ar-H), 8.69 (br. s., 2H, 2-indole-H), 8.23 (br. s., 1H, 4-Ar-H), 7.84 (br. s., 1H, 5-Ar-H), 7.75 (br. s., 2H, 4-indole-H), 7.41 (br. s., 2H, 6-indole-H), 7.18 (br. s., 2H, 5-indole-H), 6.72 (br. s., 2H, 7-indole-H). ^{13}C NMR (151 MHz, METHANOL-d$_4$) 160.6 (1C, C$^+$), 151.6 (1C), 149.1 (2C), 148.4 (1C), 140.4 (2C), 127.3 (3C), 126.0 (4C), 125.8 (2C), 123.8 (2C), 123.3 (2C), 115.0 (2C). HRMS (ESI, *m/z*) calcd for $C_{22}H_{16}N_3^+$ [M]$^+$: 322.1339, found: 322.1341.

6.1.34. Tri(1H-indol-3-yl)methylium chloride (9d)

Compound **9d** was obtained according to **general procedure 6.1.3.** 0.55 mmol Ph-C-DIM was used. Compound **9d** was obtained as red solid (201 mg, yield = 92%). HPLC purity >98%. ^{1}H NMR (600 MHz, DMSO-d_6) 13.81 (br. s., 3H, 1-indole-H), 8.40 (s, 3H, 2-indole-H), 7.75 (d, J = 8.07 Hz, 3H, 4-indole-H), 7.33 (t, J = 7.89 Hz, 3H, 6-indole-H), 7.06 (t, J = 6.88 Hz, 3H, 5-indole-H), 6.98 (br. s., 3H, 7-indole-H). ^{13}C NMR (151 MHz, DMSO-d_6) 160.9 (1C, C$^+$), 143.1 (3C), 139.5 (3C), 127.6 (3C), 125.3 (3C), 123.6 (3C), 121.7 (3C), 120.8 (3C), 114.3 (3C). HRMS (ESI, *m/z*) calcd for $C_{25}H_{18}N_3^+$ [M]$^+$: 360.1495, found: 360.1495.

6.1.35. Benzo[c]thiophen-1-yldi(1H-indol-3-yl)methylium chloride (9e)

Compound **9e** was obtained according to **general procedure 6.1.3.** 1 mmol Ph-C-DIM was used. Compound **9e** was obtained as red solid (206 mg, yield = 50%). HPLC purity >98%. ^{1}H NMR (600 MHz, DMSO-d_6) 14.16 (br. s., 2H, 1-indole-H), 8.76 (br. s., 2H, 2-indole-H), 8.61 (s, 1H, 2-Ar-H), 8.27 (d, J = 8.25 Hz, 1H, 4-Ar-H), 7.72 (d, J = 8.07 Hz, 2H, 4-indole-H), 7.47 (t, J = 8.16 Hz, 1H, 6-Ar-H), 7.37 (d, J = 7.34 Hz, 2H, 6-indole-H), 7.20—7.27 (m, 2H), 7.09 (br. s., 2H), 6.63 (br. s, 2H, 7-indole-H). ^{13}C NMR (151 MHz, DMSO-d_6) 160.41 (1C, C$^+$), 147.28 (2C), 140.74 (2C), 140.14 (2C), 126.95 (1C), 126.21 (4C), 126.10 (2C), 124.81 (2C), 124.16 (2C), 123.27 (2C), 121.99 (1C), 121.30 (2C), 114.97 (2C). HRMS (ESI) calcd for $C_{25}H_{17}N_2S^+$[M]$^+$: 377.1107, found: 377.1109.

6.1.36. Di(1H-indol-3-yl)(6-(trifluoromethyl)pyridin-3-yl) methylium chloride (9f)

Compound **9f** was obtained according to **general procedure 6.1.3.** 0.38 mmol Ph-C-DIM was used. Compound **9f** was obtained as red solid (130 mg, yield = 80%). HPLC purity >98%. ^{1}H NMR (600 MHz, DMSO-d_6) 14.60 (br. s., 2H, 1-indole-H), 8.98 (br. s., 1H, 2-Ar-H), 8.70 (br. s., 2H, 2-indole-H), 8.40 (br. s., 1H, 6-Ar-H), 8.23 (br. s., 1H, 5-Ar-H), 7.78 (d, J = 4.40 Hz, 2H, 4-indole-H), 7.45 (br. s., 2H, 6-indole-H), 7.22 (br. s., 2H, 5-indole-H), 6.76 (br. s., 2H, 7-indole-H). ^{13}C NMR (151 MHz, DMSO-d_6) 162.3 (1C, C$^+$), 152.6 (1C), 149.1 (q, $J_{C\text{-}F}$ = 34.1 Hz, 1C, 4-Ar-C), 148.3 (2C), 142.9 (1C), 139.8 (2C), 126.1

(2C), 125.6 (2C), 124.6 (2C), 121.7 (2C), 121.6 (1C), 121.4 (q, J_{C-F} = 274.0 Hz, 1C, $-CF_3$), 121.0 (2C), 120.9 (1C), 114.7 (2C). HRMS (ESI, *m/z*) calcd for $C_{23}H_{15}F_3N_3^+[M]^+$: 390.1213, found: 390.1207.

6.1.37. Bis(1-methyl-1H-indol-3-yl)(4-(trifluoromethyl)phenyl) methylium methanesulfonate (10a)

Compound **10a** was obtained according to **general procedure 6.1.3.** 2.5 mmol Ph-C-DIM was used. Compound **10a** was obtained as red solid (909 mg, yield = 71%). HPLC purity >98%. ^{1}H NMR (600 MHz, DMSO-d_6) 8.74 (br. s., 2H, 2-indole-H), 8.07 (d, *J* = 8.07 Hz, 2H, 3,5-Ar-H), 7.90 (d, *J* = 7.89 Hz, 2H, 2,6-Ar-H), 7.87 (d, *J* = 8.07 Hz, 2H, 4-indole-H), 7.51 (t, *J* = 7.61 Hz, 2H, 6-indole-H), 7.26 (t, *J* = 7.61 Hz, 2H, 5-indole-H), 6.71 (br. s., 2H, 7-indole-H), 4.13 (s, 6H, $-CH_3$), 2.30 (s, 3H, $-SO_3$-CH_3). ^{13}C NMR (151 MHz, DMSO-d_6) 164.6 (1C, C^+), 150.2 (2C), 140.4 (2C), 133.8 (1C), 132.5 (q, J_{C-F} = 29.7 Hz, 1C, 4-Ar-C), 126.3 (2C), 126.1 (4C), 125.1 (4C), 124.0 (q, J_{C-F} = 272.9 Hz, 1C, $-CF_3$), 121.5 (2C), 120.2 (2C), 113.3 (2C), 35.0 (2C). HRMS (ESI) calcd for $C_{26}H_{20}F_3N_2^+[M]^+$: 417.1573, found: 417.1570.

6.1.38. (1-methyl-1H-indol-3-yl)(1H-indol-3-yl)(4-(trifluoromethyl)phenyl)methylium methanesulfonate (10b)

Compound **10b** was obtained according to **general procedure 6.1.3.** 0.74 mmol Ph-C-DIM was used. Compound **10b** was obtained as red solid (287 mg, yield = 78%). HPLC purity >98%. ^{1}H NMR (600 MHz, DMSO-d_6) 14.07 (br. s., 1H, 1-indole-H), 8.78 (br. s., 1H, 2-indole-H), 8.69 (br. s., 1H, 2′-indole-H), 8.07 (d, *J* = 8.07 Hz, 2H, 3,5-Ar-H), 7.91 (d, *J* = 8.07 Hz, 2H, 2,6-Ar-H), 7.87 (d, *J* = 8.25 Hz, 1H, 4-indole-H), 7.75 (d, *J* = 8.07 Hz, 1H, 4′-indole-H), 7.51 (t, *J* = 7.61 Hz, 1H, 6-indole-H), 7.42 (t, *J* = 7.61 Hz, 1H, 6′-indole-H), 7.27 (t, *J* = 7.61 Hz, 1H, 5-indole-H), 7.18 (t, *J* = 7.61 Hz, 1H, 5′-indole-H), 6.67 (br. s., 2H, 7,7′-indole-H), 4.13 (s, 3H, $-CH_3$), 2.34 (s, 3H, $-SO_3$-CH_3). ^{13}C NMR (151 MHz, DMSO-d_6) 165.64 (1C, C^+), 150.8 (1C), 147.6 (1C), 140.6 (1C), 140.0 (1C), 133.0 (1C), 132.6 (q, J_{C-F} = 33.0 Hz, 1C, 4-Ar-C), 127.1 (1C), 126.9 (1C), 126.7 (1C), 126.6 (3C), 126.5 (1C), 125.3 (1C), 124.5 (1C), 123.5 (q, J_{C-F} = 274.0 Hz, 1C, $-CF_3$), 121.9 (2C), 121.2 (1C), 120.6 (1C), 114.6 (1C), 113.4 (1C), 39.1 (1C), 35.0 (1C). HRMS (ESI) calcd for $C_{25}H_{18}F_3N_2^+[M]^+$: 403.1417, found: 403.1412.

6.1.39. (1-ethyl-1H-indol-3-yl)(1H-indol-3-yl)(4-(trifluoromethyl) phenyl)methylium chloride (10c)

Compound **10c** was obtained according to **general procedure 6.1.3.** 0.50 mmol Ph-C-DIM was used. Compound **10c** was obtained as red solid (206 mg, yield = 91%). HPLC purity >98%. ^{1}H NMR (600 MHz, DMSO-d_6) 14.51 (br. s., 1H, 1-indole-H), 8.83 (br. s., 1H, 2-indole-H), 8.75 (br. s., 1H, 2′-indole-H), 8.07 (d, *J* = 7.89 Hz, 2H, 3,5-Ar-H), 7.87–7.96 (m, 3H), 7.75 (d, *J* = 7.70 Hz, 1H, 4′-indole-H), 7.48 (t, *J* = 7.52 Hz, 1H, 6-indole-H), 7.41 (t, *J* = 7.34 Hz, 1H, 6′-indole-H), 7.24 (t, *J* = 7.43 Hz, 1H, 5-indole-H), 7.18 (t, *J* = 7.24 Hz, 1H, 5′-indole-H), 6.65 (br. s., 2H, 7,7′-indole-H), 4.54 (q, *J* = 6.97 Hz, 2H, $-CH_2$-), 1.56 (t, *J* = 7.15 Hz, 3H, $-CH_3$). ^{13}C NMR (151 MHz, DMSO-d_6) 165.5 (1C, C^+), 149.2 (1C), 148.1 (1C), 140.1 (1C), 139.6 (1C), 133.4 (1C), 132.5 (q, J_{C-F} = 33.0 Hz, 1C, 4-Ar-C), 126.8 (1C), 126.7 (1C), 126.2 (4C), 126.1 (1C), 126.0 (1C), 124.8 (1C), 124.6 (1C), 123.9 (q, J_{C-F} = 274.0 Hz, 1C, $-CF_3$), 121.5 (2C), 121.2 (1C), 120.5 (1C), 114.8 (1C), 113.4 (1C), 43.1 (1C), 14.6 (1C). HRMS (ESI, *m/z*) calcd for $C_{26}H_{20}F_3N_2^+[M]^+$: 417.1573, found: 417.1577.

6.1.40. (1H-indol-3-yl)(1-propyl-1H-indol-3-yl)(4-(trifluoromethyl)phenyl)methylium chloride (10d)

Compound **10d** was obtained according to **general procedure 6.1.3.** 0.46 mmol Ph-C-DIM was used. Compound **10d** was obtained as red solid (159 mg, yield = 74%). HPLC purity >98%. ^{1}H NMR (600 MHz, DMSO-d_6) 14.45 (br. s., 1H, 1-indole-H), 8.73 (br. s., 2H, 2,2′-indole-H), 8.04 (br. s., 2H, 4,4′-indole-H), 7.91–7.95 (m, 1H), 7.88 (br. s., 2H, 3,5-Ar-H), 7.73 (br. s., 1H), 7.34–7.55 (m, 2H, 2,6-Ar-H), 7.02–7.31 (m, 2H), 6.46–6.87 (m, 2H), 4.06 (br. s., 2H, -N-CH_2-), 1.12–1.36 (m, 3H, $-CH_3$), 0.94 (br. s., 2H, $-CH_2$-). ^{13}C NMR (151 MHz, DMSO-d_6) 165.7 (1C, C^+), 149.5 (1C), 149.5 (1C), 147.8 (1C), 139.7 (1C), 139.6 (1C), 133.2 (1C), 132.8 (q, *J* = 33.01 Hz, 1C, -C-CF_3), 126.5 (1C), 126.1 (1C), 126.0 (3C), 125.9 (2C), 124.9 (1C), 124.5 (1C), 124.01 (q, *J* = 275.10 Hz, 1C, $-CF_3$), 121.3 (1C), 121.1 (1C), 120.4 (1C), 120.3 (1C), 114.6 (1C), 113.3 (1C), 47.5 (1C), 19.2 (1C), 13.4 (1C). HRMS (ESI) calcd for $C_{27}H_{22}F_3N_2^+[M]^+$: 431.1730, found: 431.1735.

6.1.41. (1-butyl-1H-indol-3-yl)(1H-indol-3-yl)(4-(trifluoromethyl) phenyl)methylium chloride (10e)

Compound **10e** was obtained according to **general procedure 6.1.3.** 0.24 mmol Ph-C-DIM was used. Compound **10e** was obtained as red solid (96 mg, yield = 82%). HPLC purity >98%. ^{1}H NMR (600 MHz, DMSO-d_6) 14.63 (br. s., 1H, 1-indole-H), 8.84 (br. s., 1H, 2-indole-H), 8.71 (br. s., 1H, 2′-indole-H), 8.07 (d, *J* = 7.89 Hz, 2H, 3,5-Ar-H), 7.93 (d, *J* = 8.25 Hz, 1H, 4-indole-H), 7.91 (d, *J* = 7.70 Hz, 2H, 2,6-Ar-H), 7.77 (d, *J* = 8.07 Hz, 1H, 4′-indole-H), 7.48 (t, *J* = 7.52 Hz, 1H, 6-indole-H), 7.41 (t, *J* = 7.34 Hz, 1H, 6′-indole-H), 7.24 (t, *J* = 7.52 Hz, 1H, 5-indole-H), 7.18 (t, *J* = 7.43 Hz, 1H, 5′-indole-H), 6.66 (br. s., 2H, 7,7′-indole-H), 4.51 (t, *J* = 7.06 Hz, 2H, -N-CH_2-), 1.94 (m, 2H, -N-C-CH_2-), 1.39 (m, 2H, $-CH_2$-CH_3), 0.95 (t, *J* = 7.34 Hz, 3H, $-CH_3$). ^{13}C NMR (151 MHz, DMSO-d_6) 165.8 (1C, C^+), 149.6 (1C), 148.0 (1C), 140.0 (1C), 139.7 (1C), 133.9 (1C), 132.5 (q, J_{C-F} = 33.0 Hz, 1C, 4-Ar-C), 126.7 (1C), 126.2 (5C), 126.1 (1C), 126.0 (1C), 125.9 (1C), 124.9 (1C), 123.9 (q, J_{C-F} = 274.2 Hz, 1C, $-CF_3$), 121.5 (2C), 121.4 (1C), 120.3 (1C), 114.7 (1C), 113.5 (1C), 47.7 (1C), 31.0 (1C), 19.4 (1C), 13.5 (1C). HRMS (ESI, *m/z*) calcd for $C_{28}H_{24}F_3N_2^+[M]^+$: 445.1886, found: 445.1889.

6.1.42. (1H-indol-3-yl)(1-pentyl-1H-indol-3-yl)(4-(trifluoromethyl) phenyl)methylium chloride (10f)

Compound **10f** was obtained according to **general procedure 6.1.3.** 0.24 mmol Ph-C-DIM was used. Compound **10f** was obtained as red solid (104 mg, yield = 87%). HPLC purity >98%. ^{1}H NMR (600 MHz, DMSO-d_6) 14.59 (br. s., 1H, 1-indole-H), 8.84 (br. s., 1H, 2-indole-H), 8.71 (br. s., 1H, 2′-indole-H), 8.07 (d, *J* = 8.07 Hz, 2H, 3,5-Ar-H), 7.94 (s, 1H, 4-indole-H), 7.91 (d, *J* = 7.89 Hz, 2H, 2,6-Ar-H), 7.77 (d, *J* = 7.15 Hz, 1H, 4′-indole-H), 7.48 (t, *J* = 7.61 Hz, 1H, 6-indole-H), 7.41 (t, *J* = 7.61 Hz, 1H, 6′-indole-H), 7.24 (t, *J* = 7.52 Hz, 1H, 5-indole-H), 7.18 (t, *J* = 7.34 Hz, 1H, 5′-indole-H), 6.67 (br. s., 2H, 7,7′-indole-H), 4.50 (t, *J* = 7.06 Hz, 2H, -N-CH_2-), 1.95 (m, 2H, -N-C-CH_2-), 1.36 (m, 4H), 0.84–0.94 (m, 3H, $-CH_3$). ^{13}C NMR (151 MHz, DMSO-d_6) 166.1 (1C, C^+), 149.7 (1C), 148.0 (1C), 139.9 (2C), 132.8 (q, J_{C-F} = 29.2 Hz, 1C, 4-Ar-C), 129.2 (1C), 126.8 (1C), 126.4 (2C), 126.3 (5C), 125.4 (1C), 125.0 (1C), 124.0 (q, J_{C-F} = 274.2 Hz, 1C, $-CF_3$), 121.6 (2C), 121.3 (1C), 120.8 (1C), 114.9 (1C), 113.7 (1C), 48.1 (1C), 28.8 (1C), 28.4 (1C), 21.9 (1C), 14.0 (1C). HRMS (ESI, *m/z*) calcd for $C_{29}H_{26}F_3N_2^+[M]^+$: 459.2043, found: 459.2048.

6.2. Biological assay

6.2.1. Cell culture

Human TNBC breast cancer cell line MDA-MB-231 and BT549, mouse embryonic fibroblast (MEF) cells and HEK293T were cultured in Dulbecco's Eagle's medium (DMEM) supplemented with 10% fetal bovine serum (FBS). Human colorectal carcinoma cancer cell line HCT116 and SW620 were cultured in RPMI-1640 supplemented 10% FBS. Normal mammary cell line MCF10A and normal colon cell line NCM460 were cultured in DMEM with 20% FBS and 10 ng/ml Epidermal Growth Factor (EGF).

6.2.2. Plasmids construction and transfection

Plasmids pcmv-myc-Nur77, pcmv-Myc-Nur77-LBD, pFlag-cmv-2-Bcl-2, pcmv-myc-Bcl-2, pEGFP-C1-Nur77, pEGFP-C1-Nur77-LBD

were constructed with standard methods as described previously [35]. Cell transfection was carried out by using lipofectamine 2000 according to the manufacture's instruction.

6.2.3. Western blotting

Cell lysates were electrophoresed by SDS-PAGE gel and transferred to polyvinylidene difluoride (PVDF) membrane. The membranes were blocked with 5% skimmed milk in TBST (50 mM Tris-HCl (pH 7.4), 150 mM NaCl and 0.1% Tween20) for 1 h at room temperature, then incubated with primary antibodies and secondary antibodies and detected using ECL system (Thermo). The dilutions of the primary antibodies were all in 1:1000.

6.2.4. Apoptosis assay

Cells plated at a density of 1×10^6 per well on six-well plates were treated with 0.5 μM of **8n** or **10b** for 6 h, and then the suspension and the adherent cells were collected, stained with Annexin V-FITC for 10 min and with propidium iodide for 5 min, and analyzed immediately by cytoFLEX Flow Cytometry System (Beckman-Coulter, Miami, FL, USA) using FITC and PC5.5.

6.2.5. CoIP assay

Cells transfected with various plasmids were lysed in lysis buffer (20 mM Tris (pH 7.5), 150 mM NaCl, 1% Triton X-100, 1 mM EDTA, 30 mM NaF, 2 mM sodium pyrophosphate) with a cocktail of proteinase inhibitors (Roche). 5% of cell lysates were taken out to represent Input. Lysates were incubated with the appropriate antibody at 4°Cfor 12 h and subsequently incubated with protein A-Sepharose beads for 3 h. Then collect the immunoprecipitants at 3000 rpm and washed three times with PBS. The protein—antibody complexes recovered on beads were subjected to Western blotting.

6.2.6. Immunostainning

Cells incubated on glass slides were fixed in 4% paraformaldehyde overnight and permeabilized with PBS containing 0.1% Triton X-100 for 15 min on ice. Cells were blocked with PBS containing 1% bovine serum albumin (BSA) for 30 min at room temperature, and incubated with various primary antibodies at 4 °C for 12 h. Then wash the cells with PBS and incubated with secondary antibodies for another 3 h at room temperature. Mitochondria were marked by Mitotracker (Deep Red) (1: 20000 dilution) for additional 30 min before fixed in 4% paraformaldehyde. Cells were co-stained with 4′6′-diamidino-2- phenylindole (DAPI) (Sigma) for the visualization of nuclei. Fluorescent images were collected and analyzed by using a fluorescence microscopy or MRC-1024 MP laser-scanning confocal microscope (Bio-Rad, Hercules, CA).

6.2.7. Mitochondrial separation

10% of the collected cells were taken out to represent the whole cells. Resuspend other cells in solution Buffer D (10 mM Tris-HCl pH 7.5, 2 mM $MgCl_2$, 10 mM KCl, 250 mM sucrose, 0.5 mM DTT) containing a cocktail of protease inhibitors for 15 min on ice. Use a homogenizer to stick the cells for 20 times. Centrifuge at 500 g for 5 min to get supernatant S1, then centrifuge S1 at 5000 g for 10 min to get precipitate P1 as a mitochondrial component. The various fractions were analyzed by SDS-PAGE. *Anti*-PARP antibody was used to ensure the purity of nuclear. Anti-Tom20 antibody was used to detect the purity of mitochondria.

6.2.8. The cell viability assay

Cell viability was determined by the MTT assay. Cells were seeded in 96-well plates at 10^4 cells/well and then treated with various concentrations of potent compounds for 24 h. Then the cells were incubated with 5 mg/mL 3-(4,5-dimethylthiazol-2-yl)-2,5-diphenyltetrazolium bromide (MTT) for 4 h at 37 °C. MTT supernatant in each well was removed carefully, and 100 μL of DMSO was added. Absorbance was measured at 490 nm. The IC_{50} of each compound was calculated by GraphPad Prism 8.0 software.

6.2.9. Protein expression and purification

The human Nur77-LBD (367—598) was cloned as an N-terminal histidine-tagged fusion protein in pET15b expression vector and overproduced in *Escherichia coli* BL21 DE3 strain. Cells were harvested and sonicated, and the extract was incubated with the His60 Ni Superflow resin.

6.2.10. Fluorescence quenching

The binding of **8n**, **10b** and **10c** to Nur77 was measured by Varioskan scanning spectrofluorometer and spectrophotometer. In each assay, 3.0 mL portion of Nur77-LBD PBS solution (1 μM/L) was added accurately into the quartz cell and it was titrated by successive additions of a 0.01—1 μM stock solution at 25 °C. The excitation wavelength was 280 nm, and the emission measurement range was 300—500 nm. To estimate the dissociation constant (K_d), the maximum fluorescence intensities at 330 nm with increasing concentrations of compound were measured, and the values of K_d were calculated according to the reported formula [47].

6.2.11. Surface plasmon resonance (SPR)

The binding kinetics between Nur77-LBD and **8n**, **10b** and **10c** were performed on a BIAcore T200 instrument (GE Healthcare) at 25 °C. Nur77-LBD were diluted to 0.05 mg/mL in 10 mM NaAc (pH 5.0) and immobilized on a CM5 sensor chip (GE Healthcare) by amine coupling at densities ~9000 RU according to the manufacturer's instructions. Gradient concentrations of compounds were injected into the flow cells in running buffer (PBS, 0.4% DMSO) at a flow rate of 30 μL/min for 150 s of association phase followed by a 420 s dissociation phase and a 30 s regeneration phase (10 mM Glycin-HCl, pH 2.5). The data were analyzed using BIAcore T200 Evaluation Software 2.0 and referenced for blank injections and reference Surface. The dissociation constant (K_d) was fitted to the standard 1:1 interaction model and calculated using the global fitting of the kinetic data from gradient concentrations.

6.2.12. MMTV-PyMT transgenic mouse study

12-week-old female mice of a transgenic mouse on the FVB/N genetic background expressing the PyMT oncogene under the control of MMTV LTR promoter40 were randomized into different groups (n = 6) and oral gavaged with **8n** or **10b** for 14 days. **8n** and **10b** were dissolved in DMSO and diluted with normal saline containing 5.0% (V/V) Tween-80 to a final concentration 3 mg/mL. All experimentations and animal usage were performed and approved by the Animal Care and Use Committee of Xiamen University.

6.2.13. Statistical analysis

Data were expressed as mean ± SD. Each assay was repeated in triplicate in three independent experiments. The statistical significance of the differences among the means of several groups was determined using Student's t-test. Differences were considered statistically significant with $P < 0.05$.

6.2.14. In vivo pharmacokinetic (PK) profile in rats

The pharmacokinetic analysis of compound **BI1071**(**8n)** and **10b** was performed on Sprague-Dawley rats weighing between 200 and 220 g. All experiments with animals were approved by the Animal Care and Use Committee of Xiamen University, in accordance with the animal care and use guidelines. The oral dose of compounds was 5 mg/kg, and the intravenous dose was 0.5 mg/kg. Compounds were dosed as a solution in DMSO/T-80/H_2O (1 : 5: 94 by volume).

For **8n**, the rats were randomly assigned into two groups consisting of three males and three females per group, and blood samples were collected by tubes containing Na heparin (10 mg/mL, 5 μL) at 5 min, 15 min, 30 min, 45 min, 1 h, 2 h, 4 h, 8 h, 12 h, 24 h and 36 h after intravenous administered, and 1 h, 2 h, 4 h, 6 h, 8 h, 10 h, 12 h, 14 h, 24 h and 36 h after oral administered. For **10b**, the rats were randomly assigned into two groups consisting of four ones per group. Blood samples were collected by tubes containing Na heparin (10 mg/mL, 5 μL) at 5 min, 15 min, 30 min, 45 min, 1 h, 2 h, 4 h, 8 h, 12 h, 24 h and 36 h after intravenous administered, and 0.5 h, 1 h, 3 h, 4 h, 6 h, 8 h, 10 h, 12 h, 24 h and 36 h after oral administered. The bloods were centrifuged at 5000 r/min for 15 min at 4 °C to separate the plasma (50 μL). Plasma samples were added with 5 μL of 10.0 μg/mL internal standard (IS: Carbamazrpine), and vortex-mixed for 15 s, then the 445 μL methanol (2% HCl) were added into the solution and vortex-mixed for 1 min to precipitate proteins. The supernatant was collected after centrifuging at 12000 r/min for 15 min at 4 °C, filtered through a 0.22 μm filter membrane, and injected with 5 μL into the liquid chromatography tandem mass spectrometry (LC-MS/MS) system for the analysis (Waters Acquity UPLC- XEVOTQSMIC). The plasma concentration−time data of **8n** and **10b** were analyzed using the DAS 3.0 to obtain the pharmacokinetic parameters, and pharmacokinetic parameters were shown as mean ± standard deviation.

6.2.15. Molecular docking

Molecular docking was performed with Glide (Schrodinger 2019-1) using standard routine and default setting [48]. The crystal structure of Nur77-LBD in complex with THPN (PDB ID: 3V3Q) was used. Compounds were docked to protein with standard precision mode. The docking results were visualized with PyMOL (version 2.3.0, Open-Source PyMOL™ by Schrodinger) [49].

Declaration of competing interest

The authors declare that they have no known competing financial interests or personal relationships that could have appeared to influence the work reported in this paper.

7. Acknowledgement

This work was supported by the grants from the National Nature Science Fund of China (NSFC-31271453, NSFC-31471318, NSFC-91129302 and NSFC-81301888), the Fundamental Research Funds for the Central Universities (2013121038, 20720180052), the Natural Science Foundation of Fujian Province of China (No. 2018J01133).

Appendix A. Supplementary data

Supplementary data to this article can be found online at https://doi.org/10.1016/j.ejmech.2020.113020.

References

[1] K. Kurakula, D.S. Koenis, C.M. van Tiel, C.J.M. de Vries, NR4A nuclear receptors are orphans but not lonesome, BBA-Mol. Cell. Res. 1843 (2014) 2543−2555.
[2] S.E. Mullican, J.R. DiSpirito, M.A. Lazar, The orphan nuclear receptors at their 25-year reunion, J. Mol. Endocrinol. 51 (2013) 115−140.
[3] M.A. Pearen, G.E.O. Muscat, Minireview: nuclear hormone receptor 4A signaling: implications for metabolic disease, Mol. Endocrinol. 24 (2010) 1891−1903.
[4] A.A.J. Hamers, R.N. Hanna, H. Nowyhed, C.C. Hedrick, C.J.M. de Vries, NR4A nuclear receptors in immunity and atherosclerosis, Curr. Opin. Lipidol. 224 (2013) 381−385.
[5] H.Y. Won, E.S. Hwang, Transcriptional modulation of regulatory T cell development by novel regulators NR4As, Arch Pharm. Res. (Seoul) 39 (2016) 1530−1536.
[6] R. Hashida, N. Ohkura, H. Saito, G. Tsujimoto, The NR4A nuclear receptor family in eosinophils, J. Hum. Genet. 52 (2017) 13−20.
[7] C.M. van Tiel, C.J.M. de Vries, NR4All in the vessel wall, J. Steroid Biochem. 130 (2012) 186−193.
[8] Q.X. Li, N. Ke, R. Sundaram, F. Wong-Staal, NR4A1, 2, 3-an orphan nuclear hormone receptor family involved in cell apoptosis and carcinogenesis, Histol. Histopathol. 21 (2006) 533−540.
[9] H.S. Ranhotra, The NR4A orphan nuclear receptors: mediators in metabolism and diseases, J. Recept. Sig. Transd. 35 (2015) 184−188.
[10] R. Rodriguez-Calvo, M. Tajes, M. Vazquez-Carrera, The NR4A subfamily of nuclear receptors: potential new therapeutic targets for the treatment of inflammatory diseases, Expert Opin. Ther. Targets 21 (2017) 291−304.
[11] G.M. Niu, L. Lu, J. Gan, D. Zhang, J.Z. Liu, G.J. Huang, Dual roles of orphan nuclear receptor TR3/Nur77/NGFI-B in mediating cell survival and apoptosis, Int. Rev. Cel. Mol. Bio. 313 (2014) 219−258.
[12] S. Safe, U.H. Jin, E. Hedrick, A. Reeder, S.O. Lee, Minireview: role of orphan nuclear receptors in cancer and potential as drug dargets, Mol. Endocrinol. 28 (2014) 157−172.
[13] A.J.A. Deutsch, H. Angerer, T.E. Fuchs, P. Neumeister, The nuclear orphan receptors NR4A as therapeutic target in cancer therapy, Anti-Cancer Agents, Med. Chem. 12 (2012) 1001−1014.
[14] S.O. Lee, X. Li, S. Khan, S. Safe, Targeting NR4A1 (TR3) in cancer cells and tumors, Expert Opin. Ther. Targets 15 (2011) 195−206.
[15] E. Hedrick, S.O. Lee, R. Doddapaneni, M. Singh, S. Safe, Nuclear receptor 4A1 as a drug target for breast cancer chemotherapy, Endocr. Relat. Canc. 22 (2015) 831−840.
[16] S.K. Kolluri, N. Bruey-Sedano, X. Cao, B. Lin, F. Lin, Y.H. Han, M.I. Dawson, X.K. Zhang, Mitogenic effect of orphan receptor TR3 and its regulation by MEKK1 in lung cancer cells, Mol. Cell Biol. 23 (2003) 8651−8667.
[17] S.O. Lee, M. Abdelrahim, K. Yoon, S. Chintharlapalli, S. Papineni, K. Kim, H. Wang, S. Safe, Inactivation of the orphan nuclear receptor TR3/Nur77 inhibits pancreatic cancer cell and tumor growth, Canc. Res. 70 (2010) 6824−6836.
[18] S.O. Lee, T. Andey, U.H. Jin, K. Kim, M. Sachdeva, S. Safe, The nuclear receptor TR3 regulates mTORC1 signaling in lung cancer cells expressing wild-type p53, Oncogene 31 (2012) 3265−3276.
[19] H. Wu, Y.Y. Lin, W.G. Li, Z. Sun, W.W. Gao, H.P. Zhang, L. Xie, F.Q. Jiang, B. Qin, T.D. Yan, Regulation of Nur77 expression by β-catenin and its mitogenic effect in colon cancer cells, Faseb. J. 25 (2011) 192−205.
[20] H.M. Mohan, C.M. Aherne, A.C. Rogers, A.W. Baird, D.C. Winter, E.P. Murphy, Molecular pathways: the role of NR4A orphan nuclear receptors in cancer, Clin. Canc. Res. 18 (2012) 3223−3228.
[21] S.K.Y. To, J.Z. Zeng, A.S.T. Wong, Nur77: a potential therapeutic target in cancer, Expert Opin. Ther. Targets 16 (2012) 573−585.
[22] X.K. Zhang, Targeting Nur77 translocation, Expert Opin. Ther. Targets 11 (2007) 69−79.
[23] J.D. Woronicz, B. Calnan, V. Ngo, A. Winoto, Requirement for the orphan steroid-receptor Nur77 in apoptosis of T-Cell hybridomas, Nature 367 (1994) 277−281.
[24] Z.G. Liu, S.W. Smith, K.A. McLaughlin, L.M. Schwartz, B.A. Osborne, Apoptotic signals delivered through the T-Cell receptor of a T-Cell hybrid require the immediate-early gene Nur77, Nature 367 (1994) 281−284.
[25] Y. Li, B.Z. Lin, A. Agadir, R. Liu, M.I. Dawson, J.C. Reed, J.A. Fontana, F. Bost, P.D. Hobbs, Y. Zheng, G.Q. Chen, B. Shroot, D. Mercola, X.K. Zhang, Molecular determinants of AHPN (CD437)-induced growth arrest and apoptosis in human lung cancer cell lines, Mol. Cell Biol. 18 (1998) 4719−4731.
[26] Z. Sun, X. Cao, M.M. Jiang, Y. Qiu, H. Zhou, L. Chen, B. Qin, H. Wu, F. Jiang, J. Chen, J. Liu, Y. Dai, H.F. Chen, Q.Y. Hu, Z. Wu, J.Z. Zeng, X.S. Yao, X.K. Zhang, Inhibition of β-catenin signaling by nongenomic action of orphan nuclear receptor Nur77, Oncogene 31 (2012) 2653−2667.
[27] Y.Q. Zhou, W. Zhao, G.B. Xie, M.F. Huang, M.J. Hu, X. Jiang, D.Q. Zeng, J. Liu, H. Zhou, H.F. Chen, G.H. Wang, X.K. Zhang, Induction of Nur77-dependent apoptotic pathway by a coumarin derivative through activation of JNK and p38 MAPK, Carcinogenesis 35 (2014) 2660−2669.
[28] S. Ramaswamy, K.N. Ross, E.S. Lander, T.R. Golub, A molecular signature of metastasis in primary solid tumors, Nat. Genet. 33 (2003) 49−54.
[29] H. Li, S.K. Kolluri, J. Gu, M.I. Dawson, X.H. Cao, B.Z. Lin, G.Q. Chen, J.S. Lu, F. Lin, Z.H. Xie, J.A. Fontana, J.C. Reed, X.K. Zhang, Cytochrome c release and apoptosis induced by mitochondrial targeting of nuclear orphan receptor TR3, Science 289 (2000) 1159−1164.
[30] B.Z. Lin, S.K. Kolluri, F. Lin, W. Liu, Y.H. Han, X.H. Cao, M.I. Dawson, J.C. Reed, X.K. Zhang, Conversion of Bcl-2 from protector to killer by interaction with nuclear orphan receptor Nur77/TR3, Cell 116 (2004) 527−540.
[31] S.J. Dawson, N. Makretsov, F.M. Blows, K.E. Driver, E. Provenzano, J. Le Quesne, L. Baglietto, G. Severi, G.G. Giles, C.A. McLean, G. Callagy, A.R. Green, I. Ellis, K. Gelmon, G. Turashvili, S. Leung, S. Aparicio, D. Huntsman, C. Caldas, P. Pharoah, BCL2 in breast cancer: a favourable prognostic marker across molecular subtypes and independent of adjuvant therapy received, Br. J. Canc. 103 (2010) 668−675.
[32] C.M. Perou, T. Sorlie, M.B. Eisen, M. van de Rijn, S.S. Jeffrey, C.A. Rees, J.R. Pollack, D.T. Ross, H. Johnsen, L.A. Akslen, O. Fluge, A. Pergamenschikov, C. Williams, S.X. Zhu, P.E. Lonning, A.L. Borresen-Dale, P.O. Brown, D. Botstein, Molecular portraits of human breast tumours, Nature 6797 (2000) 747−752.
[33] N. Toshitsugu, N. Setsuo, S. Toshihiko, N. Shoji, Expression of bcl-2 oncoprotein in gastrointestinal and uterinecarcinomas and their premalignant lesions, Hum. Pathol. 28 (1997) 309−315.

[34] N.E.I. Langlois, J. Lamb, O. Eremin, S.D. Heys, Apoptosis in colorectal carcinoma occurring in patients aged 45 years and under: relationship to prognosis, mitosis, and immunohistochemical demonstration of p53, c-myc and bcl-2 protein products, J. Pathol. 182 (1997) 392–397.

[35] X.H. Chen, X.H. Cao, X.H. Tu, G. Alitongbieke, Z.B. Xia, X.T. Li, Z.W. Chen, M.M. Yin, D. Xu, S.J. Guo, Z.X. Li, L.Q. Chen, X.D. Zhang, D.Y. Xu, M.C. Gao, J. Liu, Z.P. Zeng, H. Zhou, Y. Su, X.K. Zhang, BI1071, a novel Nur77 modulator, induces apoptosis of cancer cells by activating the Nur77-Bcl-2 apoptotic pathway, Mol. Canc. Therapeut. 18 (2019) 886–899.

[36] R. Flaig, H. Greschik, C. Peluso-Iltis, D. Moras, Structural basis for the cell-specific activities of the NGFI-B and the Nurr1 ligand-binding domain, J. Biol. Chem. 19 (2005) 19250–19258.

[37] Y. Zhan, X. Du, H. Chen, J. Liu, B. Zhao, D. Huang, G. Li, Q. Xu, M. Zhang, B.C. Weimer, D. Chen, Z. Cheng, L. Zhang, Q. Li, S. Li, Z. Zheng, S. Song, Y. Huang, Z. Ye, W. Su, S.C. Lin, Y. Shen, Q. Wu, Cytosporone B is an agonist for nuclear orphan receptor Nur77, Nat. Chem. Biol. 4 (2008) 548–556.

[38] Y.Y. Zhan, Y. Chen, Q. Zhang, J.J. Zhuang, M. Tian, H.Z. Chen, L.R. Zhang, H.K. Zhang, J.P. He, W.J. Wang, R. Wu, Y. Wang, C. Shi, K. Yang, A.Z. Li, Y.Z. Xin, T.Y. Li, J.Y. Yang, Z.H. Zheng, C.D. Yu, S.C. Lin, C. Chang, P.Q. Huang, T. Lin, Q. Wu, The orphan nuclear receptor Nur77 regulates LKB1 localization and activates AMPK, Nat. Chem. Biol. 8 (2012) 897–904.

[39] L. Li, Y. Liu, H.Z. Chen, F.W. Li, J.F. Wu, H.K. Zhang, J.P. He, Y.Z. Xing, Y. Chen, W.J. Wang, X.Y. Tian, A.Z. Li, Q. Zhang, P.Q. Huang, J. Han, T. Lin, Q. Wu, Impeding the interaction between Nur77 and p38 reduces LPS-induced inflammation, Nat. Chem. Biol. 11 (2015) 339–346.

[40] J.B. Baell, G.A. Holloway, New substructure filters for removal of pan assay interference compounds (PAINS) from screening libraries and for their exclusion in bioassays, J. Med. Chem. 53 (2010) 2719–2740.

[41] K. Prinsen, M.M. Cona, J. Cleynhens, H. Vanbilloen, J. Li, N. Dyubankova, E. Lescrinier, G. Bormans, Y. Ni, A. Verbruggen, Synthesis and biological evaluation of 68Ga labeled bis-DOTA-3,3'-(benzylidene)-bis-(1H-indole-2-carbohydrazide) as a PET tracer for in vivo visualization of necrosis, Bioorg. Med. Chem. Lett 23 (2013) 3216–3220.

[42] M.H. Zhuo, Y.J. Jiang, Y.S. Fan, Y. Gao, S. Liu, S. Zhang, Enantioselective synthesis of triarylmethanes by chiral imidodiphosphoric acids catalyzed Friedel-Crafts reactions, Org. Lett. 16 (2014) 1096–1099.

[43] H. Wen, L. Wang, L. Xu, Z. Hao, C.L. Shao, C.Y. Wang, J. Xiao, Fluorinated alcohol-mediated SN1-type reaction of indolyl alcohols with diverse nucleophiles, Adv. Synth. Catal. 357 (2015) 4023–4030.

[44] N.A. Meanwell, Fluorine and fluorinated motifs in the design and application of bioisosteres for drug design, J. Med. Chem. 61 (2018) 5822–5880.

[45] E.P. Gillis, K.J. Eastman, M.D. Hill, D.J. Donnelly, N.A. Meanwell, Applications of fluorine in medicinal chemistry, J. Med. Chem. 58 (2015) 8315–8359.

[46] J. Hodgson, ADMET–turning chemicals into drugs, Nat. Biotechnol. 19 (2001) 722–726.

[47] Z.X. Wang, N.R. Kumar, D.K. Srivastava, A novel spectroscopic titration method for determining the dissociation constant and stoichiometry of protein-ligand complex, Anal. Biochem. 206 (1992) 376–381.

[48] R.A. Friesner, J.L. Banks, R.B. Murphy, T.A. Halgren, J.J. Klicic, D.T. Mainz, M.P. Repasky, E.H. Knoll, M. Shelley, J.K. Perry, Glide: a new approach for rapid, accurate docking and scoring. 1. Method and assessment of docking accuracy, J. Med. Chem. 47 (2004) 1739–1749.

[49] W. DeLano, The PyMOL Molecular Graphics System, DeLano Scientific, San Carlos, CA, USA, 2002, 2002.